High Content Analysis uncovers functionally relevant metastable phenotypic states in human Endothelial Cells monolayers

Francois Chesnais[1], Juliette Le Caillec[1], Errin Roy[2], Davide Danovi[2], Lorenzo Veschini[1#]

1 Vascular Cells Dynamics Lab, ACRS, Faculty of Dentistry Oral & Craniofacial Sciences, King's College London.
2 Stem Cell Hotel, Centre for Stem Cells & Regenerative Medicine, King's College London

Correspondence to lorenzo.1.veschini@kcl.ac.uk

Abstract

Endothelial cells (EC) present distinct cell properties in different tissues. Heterogeneity within the same vascular bed has been proposed to underpin emergent behaviours in EC monolayers. Quantification and functional relevance of EC phenotypic variance are challenging to assess. Here we developed a novel EC profiling tool (ECPT) to uniquely enable single EC profiling within a monolayer and providing spatial and relational information regarding cell proliferation, inter-endothelial Junctions and NOTCH activation. We used ECPT to characterise differential phenotypes in arterial, venous and microvascular EC populations. Our analysis highlighted extensive heterogeneity within individual monolayers and revealed VEGF-modulable metastability of NOTCH signalling which in turn regulates inter-endothelial junction's stability. We suggest that accounting adaptive emerging endothelial behaviours is necessary to develop specific tissue engineering approaches and identify more effective and EC-specific therapeutic targets for cardiovascular diseases and cancer.

Introduction

Endothelial cells (EC) form the inner layer of blood and lymphatic vessels and play major roles in tissue development, angiogenesis, inflammation and immune cell trafficking[1]. EC are functionally plastic and rapidly adapt to changes in the environment to preserve homeostasis. Local EC dysregulation is a hallmark of pathological states such as atherosclerosis, ischemia and cancer[2]. EC from different tissues and vascular beds (such as arteries, capillaries, veins) exhibit distinct metabolism, morphology and gene expression[3] and contribute in diverse ways to tissue development and regeneration[4,5]. It is well established that EC are phenotypically heterogenous not only among different tissues, reflecting specialised organ-specific functions[6], but also within the same tissue. Pools of EC substitute senescent cells, maintaining endothelial homeostasis; the role of endothelial progenitor cells with high repopulating potential has been highlighted, in particular in large vessels endothelia[7]. Inter-endothelial adherens junctions (IEJ) are dynamically regulated by VE cadherin (VEC) shuffling between the cell membrane and intracellular compartments. This process presents variations across vascular beds[3] and involves molecular mechanisms including VEGF receptors, cytoskeletal proteins and NOTCH family members. VEC and NOTCH signalling are well studied in angiogenesis and development. Nonetheless, defining the role of these molecular mechanisms in EC monolayer maintenance is key to understand vessel homeostasis in different organs in the human body. Understanding the heterogeneity of EC will also have important implications to realise the full potential of tissue engineering[8]. So far, a comprehensive analysis of EC cultures exploring and quantifying phenotypic variance has proven prohibitively difficult because of lack of adequate tools.

Single cell analysis is important to identify and characterise intermediate cell states[9,10] and to demonstrate correspondence between phenotypes and function[11] despite challenges in discriminating functional phenotypes variance from biological noise[12]. Single cell transcriptomic data is becoming available (mostly in mouse[13]) and could in principle advance the characterisation of human EC [14] and provide an overview of molecular processes in distinct EC populations. Nonetheless, spatial information is essential to map variable phenotypes to function and is also required to understand higher-level functions depending on cell-cell

connectivity. Of note, cell cycle and rapid adaptative phenomena, such as immediate increase of endothelial permeability upon VEGF stimulation, rely on built-in sensing mechanisms that depend on cell-cell interaction[15]. The study of human EC models has largely concentrated on single cells, due to the limited availability of tools to study interactions at the population level. Importantly, EC monolayers maintain their integrity over years while exerting a variety of system-level functions which are emerging properties of cells in contact[16]. It has been in fact proposed that endothelial adaptability and diversity of functions within an EC population depends on cell heterogeneity[17].

Here, we present a novel comprehensive high-content analysis (HCA) platform to characterise single EC within an endothelial monolayer capturing a wealth of cell features, context features and subcellular features including extensive analysis of IEJ. This unbiased approach allows quantification of EC diversity and feature variance comprehensively[12]. We set up an endothelial cell profiling tool (ECPT) based on image analysis. Using an innovative machine learning based method (Appendix 1), we addressed automated and accurate classification of IEJ using junctional VEC immunostaining, and evaluation of NOTCH activation at the single cell level. In total, we present here data from 4 independent acquisitions in triplicate technical replicates detailing >7.5 M cell objects from >100,000 cells and >6000 images on a 29-dimensional parameter space. This approach demonstrates the feasibility of using ECPT as an exploratory platform to quantify heterogeneity in EC.
We take advantage of ECPT to address whether intermediate EC phenotypes exist within homogeneous EC populations and whether these are functionally relevant. Single EC profiling at such scale have not been reported and we here demonstrate its validity to uncover key relationships across features and to comprehensively characterise cell behaviour across distinct EC types.

Results:

HUVEC, HAoEC and HPMEC present heterogeneous phenotypes and subpopulations can be clustered by automated analysis

While heterogeneity of EC has been proposed, there are few examples of studies that achieved successful quantification phenotypic variance of EC within the same vascular bed by transcriptomic analysis[18]. We previously reported the value of specific VEC and NOTCH quantification to benchmark EC in intact monolayers[19] and we now extended our observations including relational information between individual cells which are impossible to retrieve with current single cell transcriptomic analysis.
Here, we seeded primary HUVEC, HAoEC and HPMEC under low FBS conditions for 48 hours in the absence or presence of supra-physiologic VEGF. We aimed for sufficient cells to reach confluency upon adhesion and spreading (~24 h) and we cultured for a further 24 h to enable formation of stable IEJ. EC demonstrate a uniform cobblestone morphology under low magnification, confirming monolayer stabilisation. In analysing these cultures, we focussed on proliferation, junctions and NOTCH activation. We stained for VEC, activated NOTCH (NICD), actin cytoskeleton and nuclei. Qualitative inspection at high magnification revealed remarkable morphological differences between the three cell types in culture. HUVEC appear smaller and display a relatively disorganised cytoskeleton (Supplementary Figure 1); HPMEC in contrast are largest and often demonstrate cortical distribution of the cytoskeleton; HAoEC show irregular shapes and sizes and often present as cells with stress fibres (Supplementary Figure 1).

Altogether these qualitative observations point to a complex interplay of proliferation, IEJ and NOTCH that mirrors only in part previous studies referring to EC heterogeneity and distinct traits[3,19,20]. Measuring and scoring individual EC phenotypes to demonstrate, explain and quantify EC heterogeneity at single cell resolution is a prohibitively tedious and biased approach if not automated. Therefore, we set to assemble a dedicated automated platform that can seamlessly and comprehensively quantify variance of phenotypic parameters in EC

111 in appropriate multidimensional space to ultimately define specific cell populations. To serve
112 this purpose, we developed a method to profile EC phenotypes at single cell level based on
113 extracted HCA-features, Endothelial Cell Profiling Tool (ECPT, Figure 1 and Appendix 1).
114
115 A list of 29 features extending and refining our previous proof-of-principle efforts[19] was chosen
116 including proliferation and context feature and machine learning-aided classification of
117 junctions and of NOTCH activation.
118 We resourced to tSNE based dimensionality reduction techniques to capture variance within
119 our multivariate datasets and to identify discrete populations among heterogeneous cells. We
120 first asked whether the three EC cell types analysed cluster using the chosen features. EC
121 from different cell types formed distinct clusters (Supplementary Figure 2A) suggesting that
122 our parameters of choice (Supplementary Table 1) capture key differences in the three EC
123 populations. Nonetheless, similarities across the populations are also observed (e.g., mean
124 VEC intensity, Supplementary Figure 2B).
125
126 Altogether, tSNE enabled us to (1) specify diversities between EC populations and (2)
127 demonstrate a remarkable heterogeneity within the same populations. To understand the
128 origin of this heterogeneity we dissected individual sets of features dependent on the same
129 biological mechanism. To subset our database according to tSNE clustering we also
130 developed a dedicated open-source Shiny app (https://shiny.rstudio.com) allowing interactive
131 and iterative selection of single cells or groups of cells on tSNE scatterplots. To understand in
132 detail phenotypic differences, we proceeded with the exploration of features focussing on
133 selected traits to quantify variance in proliferation, junction stability and NOTCH activation.
134
135 **Variance in proliferation: HUVEC, HAoEC and HPMEC present different proliferation**
136 **potential validated by context features**
137 By culturing HUVEC, HAoEC and HPMEC under the same standardised conditions, we
138 noticed that the three EC types present different intrinsic proliferation rates. We quantified
139 proliferating cells within the different EC types using ECPT (Figure 2B, C Supplementary
140 Figure 3). Proliferation rate was higher in HAoEC than in HUVEC at baseline (average 13.61
141 vs 11.72 % of dividing cells per field) and lower in HPMEC (average 6.81%). VEGF induced
142 a small increase in proliferation rate in all EC. We then asked whether EC proliferation was
143 mostly due to clonal proliferation as suggested[7,21] or whether EC were retaining general
144 proliferation potential and how this might differ in distinct EC cell types. In previous work form
145 our group we demonstrated that the tendency to form colonies in hiPSC correlates with
146 differential gene expression programs[22]. Following a similar strategy and the method
147 described below and in Supplementary Figure 4 we evaluated the tendency to form densely
148 packed cell clusters as a proxy of EC clonal proliferation. We developed a novel measure of
149 nuclei clustering as a proxy of clonal proliferation based on the assumption that fast
150 proliferating clones will group with reduced cytoplasm and reduced internuclear distance
151 (Supplementary Figure 4). We extracted subsets of cells by manual annotation of plots of
152 interest (Figure 1D, Appendix 1) and explored further subsets of the database according to six
153 clusters identified by tSNE (Figure 3A).
154 Figure 3B shows the mapping of the nuclei clustering index (NCI, defined as the number of
155 nuclei within a distance less than ~1/3 the mean cell diameter, Appendix 1). In other words,
156 within our definitions an NCI equal or above 2 indicates that a cell has two or more very close
157 neighbours, and this is strongly indicative that the cell resides within a group of packed cells
158 (Supplementary Figure 4). We then calculated average second cell neighbour distance
159 measurements for each cluster and found that the cells within clusters 1 and 2 had the lowest
160 average distance to second neighbours, those in cluster 3 and 5 an intermediate average
161 distance and clusters 4 and 6 were the most distanced cells (Figure 3F). Therefore, cells in
162 tSNE clusters 1 and 2 displayed both nuclei clustering and decreased 2nd neighbour distance
163 indicating that cells within these clusters are more closely packed than the rest of the
164 population. Since closely packed cells reflect compact colonies, we asked whether these
165 colonies might represent highly proliferative subclones. Figure 3D shows mapping of

proliferating cells on the tSNE plot and it appears that cells in compact colonies (clusters 1 and 2) have a higher frequency of proliferating cells. Subsequently, we calculated enrichment of dividing cells in the tSNE clusters. We found that LM cells were enriched in clusters 1 and 2 and G2/M cells in clusters 3 and 4 (Figure 3C, D). This validated our observations. Notably, cluster 3 also contained cells with a nuclei clustering index >2 (Figure 3B), had decreased 2nd neighbour distance, albeit higher than cluster 1 and 2, and an increased frequency of LM cells. Furthermore, cluster 3 and 4 contains >95% of all G2/M cells whereby cells in cluster 4 have both high 2nd neighbour distance and a nuclei clustering index <2. The same pattern was observed in all EC lines when analysed individually (Supplementary Figure 5A).
Overall, this data demonstrates that 1) highly proliferating EC clones exist within EC monolayers (clusters 1, 2 and 3) and 2) that clonal proliferation is not the only modality of EC proliferation, as isolated G2/M and LM cells were also found scattered throughout the monolayers (clusters 4, 5 and 6), (Figure 3C-F).
When we looked at differences between HAoEC, HPMEC and HUVEC we found that all cells examined had the capacity to proliferate both within colonies and in isolation. Furthermore, proliferation in isolation was more frequent than in colonies in all cell populations examined (Supplementary Figure 5B). Overall, all the EC lines we cultured continued proliferating up to 8 passages with little signs of clonal proliferation (i.e., sparse EC from all lines proliferated homogeneously, not shown). Although few seemingly highly proliferative clusters were identifiable, dividing cells were mostly found interspersed with quiescent cells within stabilised monolayers in all cell lines (Supplementary Figure 5B) suggesting that proliferative capacity is largely retained across the EC monolayers, including HPMEC which are more specialised and can proliferate, albeit at a reduced rate.

Distinct EC types display heterogeneous activation states

The evaluation of EC activation state has been previously based on actin cytoskeleton organisation[23] (Supplementary Figure 1). EC with stress fibres have been considered motile/migratory while those in which peripheral cytoskeleton overlap with cell junctions are considered quiescent. The former EC phenotypes are usually associated with cell elongation and unstable IEJ.
In line with previous observations[19], VEGF induced elongation in all cells examined (Supplementary Figure 6). At simple microscopic observation, HPMEC homogeneously demonstrated features of quiescence such as cortical cytoskeleton supporting stable junctions and surprisingly despite evidence of cell elongation VEGF did not evidently affect junctional stability in HPMEC. HAoEC and HUVEC instead presented a more heterogeneous phenotype, appeared more active and chronic VEGF treatment promoted migratory phenotypes in both cell types. Furthermore, VEGF treatment induced more stress fibres in HAoEC but not in HUVEC in contrast to previous observations under acute VEGF stimulation[24]. To substantiate these observations, we measured EC activation by ECPT. To this purpose, we trained a machine-learning based software (Cell Profiler Analyst, CPA based on fast gentle boosting) to classify quiescent, activated or stressed EC (Figure 4A, Supplementary Figure 7, Appendix 1). Under this classification, 40.6 % of HPMEC were quiescent cells, substantially more than HAoEC (20.5%) and HUVEC (16.2%). An opposite trend was observed for stressed cells (HAoEC, 25.4%; HPMEC, 13.7%; HUVEC 23.2%). VEGF had opposite effects on HAoEC and HUVEC, quiescent cells were reduced (-8.2%) in HAoEC and increased (+4%) in HUVEC while stressed cells were increased in HAoEC (+5.3%) and reduced it in HUVEC (-7.1%), (Figure 4B, Supplementary figure 7). VEGF treatment had little effects on HPMEC overall quiescence save a small increase in quiescent cells (+2.2%).
Dividing (Late mitotic) cells, as shown in Figure 2A were binned in a specific category which was used to refine cell cycle analysis based on DNA intensity (Appendix 1) overcoming a specific limitation of previous approaches[25]. Overall, these data demonstrate that HPMEC largely do not acquire a migratory phenotype and tend to be more quiescent than HAoEC and HUVEC. Chronic supra physiologic VEGF treatment increased the proportion of activated HAoEC yet interestingly it promoted quiescence in the two other EC lines analysed (Supplementary Figure 7) suggesting that the effects of VEGF are context specific.

Furthermore, all EC populations had a significant proportion (46.1-55.6%) of activated cells (i.e., an intermediate, neither migratory nor quiescent and non-proliferating, state characterised by reduced connectivity) further demonstrating that EC monolayers are composed of heterogeneous EC.

Variance in junctions: EC from different vessels display heterogeneous junction composition

IEJ morphology is an immediate index of EC activation in contrast to quiescence. In general, quiescent EC (i.e., non-proliferating, non-migrating) are also those with stabilised IEJ while migrating or proliferating EC demonstrate jagged or discontinuous junctions[23,26]. Average population measurements have been used by us and others[19,24,27] to assess stability of EC monolayers which in turn correlate with functions such as trans-endothelial permeability to large proteins[28].

Assessing IEJ at the single cell level is key to highlight subtle nuances in inter-endothelial cells connectivity within the same monolayer. Nonetheless, measuring and classifying junctional signal by image analysis is technically challenging and no currently available software is able to evaluate multiple images in a standardised way[29,30]. To overcome this obstacle, we have implemented within ECPT a junction analysis method (Appendix 1). Our method subdivides the junctional inter-cellular space in several discrete areas scored using an expert-trained machine learning algorithm (CPA with Fast gentle Boosting, Appendix 1). In line with the literature in the field, we classified each junction binning in three categories: jagged, linear or stabilised (Figure 5A). Stabilised junctions are visually reminiscent of the reticular junctions previously described[26]. To facilitate data representation, we calculated a single continuous measure accounting for the proportions of different IEJ categories (junctional stability index, STB Index, Appendix 1).

Comparing Figure 1E (tSNE mapping of the three EC lines) with Figure 5B (tSNE mapping of STB Index) it appears that the different EC lines map on areas with different STB Index a large proportion of HPMEC mapped to area with high STB Index indicating that their junctions are mostly composed of stabilised and linear junctions in contrast to the other two lines where junction's composition was very heterogeneous. To quantify differences, we evaluated the density distribution of the STB index across the three cell types (Figure 5C). It is evident that both HAoEC and HUVEC are very heterogeneous in respect to IEJ, and that many cells have a composition of different junctions. The mean STB Index was -4.7 (62.1 median IQR) for HAoEC (prevalence of linear junctions) and -23 (64.6 median IQR) for HUVEC (mixture of jagged and linear junctions). In contrast, HPMEC had prevalence of linear and stabilised junctions (30 mean) and were more homogeneous (44.2 median IQR).

Chronic exposure to 50ng/ml VEGF increased STB index in all cells to different extents (+2.2, +5.6 and +16.2 in HAoEC, HPMEC and HUVEC respectively), HPMEC junctions were also more homogeneous upon VEGF treatment (36.9 median IQR) (Figure 5C).

In vitro conditions might not support full stabilisation of IEJ therefore these results should be interpreted as differences in intrinsic EC potential to form stable monolayers in contrast to plastic but unstable (and potentially leaky) ones, rather than a faithful reflection of *in vivo* reality. Within these limitations, our results demonstrate that HPMECs' junctions are intrinsically more stable producing homogeneously stable monolayers in contrast to HAoEC and HUVEC which tend to form heterogeneous and less stable monolayers which is compatible with their differential functions, i.e., a reduced requirement to tightly regulate paracellular transit in EC from large vessels.

Variance in NOTCH activation: Quantification of NOTCH activation in EC monolayers highlights metastable cell states

In line with previous results on HEY1/HEY2 expression in HUVEC[31], we hypothesised that EC within monolayer would have a homogeneous level of NOTCH signalling either low/absent in venous EC (HUVEC) and high in arterial EC as high NOCTH signalling is associated with the

arterial phenotype[32]. One previous study has reported appreciable baseline NICD levels in HPMEC by western blotting[33] but not in comparison with other EC lines.

Computational models of NOTCH signalling pathway dynamics suggest that the NOTCH system can generate either mono-stable, bi-stable or unstable/metastable phenotypes. Unstable/metastable dynamics have never been described in EC[34,35,36]. A bi-stable scenario would entail that most non-dividing cells in a monolayer will be either NOTCH active or non-active which should promote formation of regular patterns of ON and OFF cells (Figure 6A). Conversely, if the system cannot reach a stable equilibrium (non-stability, metastability), we would expect to observe distribution between different activation states including cells without NICD (NOTCH OFF), actively signalling cells with varying NICD levels and cells with high nuclear NICD (NOTCH ON) (Figure 6A).

In order to distinguish between these possibilities, we measured the amount of NICD puncta in the cytoplasm and nuclei of single EC using ECPT. Figure 6B shows the distribution of NOTCH among four classes derived from cytoplasmic and nuclear NOTCH puncta measurements. The thresholds were selected empirically, <50 total NICD intensity reflects presence of 1-5 NICD puncta, in comparison, most highly active cells had ~50-80 NICD puncta and ~1600 total NICD intensity (Figure 6C, Appendix 1). Interestingly, we found a continuous nuance of differential NICD intensities across this range (0-~1600, Fig 6C). Our results indicate that irrespectively of origin, EC within monolayers are heterogeneous in NOTCH activation (Classification in Figure 6B). In line with current literature, HUVEC demonstrated higher degree of inactive cells (OFF) and lower percentage of highly active and ON cells (Figure 6B, Supplementary Figure 8) in comparison to HAoEC and HPMEC. NOTCH activity in pulmonary microvascular EC has not been compared to other EC previously, we found that HPMEC had the highest degree of high NOTCH highly active (~31.3%) and ON cells (~17.7%) among the EC types examined (Supplementary Figure 8). Interestingly, all EC had a significative presence of all four categories including relevant portions of “ON” and “OFF” cells demonstrating that the system is not mono-stable (Fig 6A). Analysis of static images cannot provide information regarding the exact dynamics of the system, nonetheless NICD staining conveys a temporal information as NICD puncta are necessarily indicating previous signalling from neighbouring cells and they are inherently fated to translocate to the nucleus or to be degraded before reaching the nucleus. When we plotted the distribution of all cells across nuclear to cytoplasm NICD ratio (Figure 6D and Supplementary Figure 9), we observed two peaks corresponding to OFF and ON cells and a significant proportion of cells with intermediate states including cells with significant nuclear NICD and further ongoing signalling in the cytoplasm. Qualitative inspection of the plots in Figure 6D and Supplementary Figure 9 immediately shows that 1) the plots are only compatible with unstable/metastable cell states at the population level (Figure 6A) and 2) all EC examined follow a similar pattern suggesting that NOTCH metastability might be a general feature of endothelia.

To assess the functional relevance of this phenomenon we evaluated correlations between differential NOTCH activation states and the phenotypical features described in previous results. NOTCH activation has been associated with increased junctional stability in EC[37]. When we examined correlation between NOTCH activity and junction stability at the single cell level, we did not find any evidence of correlation between the two phenomena (Supplementary Figure 10,11). Therefore, high level of NICD does not appear to affect Junctional stability within the same (receiver) cell. We then moved our focus on cell neighbourhoods by calculating field averaged measures of Junctional stability index and the frequency of NICD classes (OFF, Low, High, or ON) and we found that the average stability index increased in fields with high frequency of High cells and decreased in fields with high frequency of Low cells (Figure 7 A and Supplementary Figure 8). Overall, our data suggest that sustained NOTCH signalling in one cell favours junctional stabilisation in its neighbourhood while low levels of NOTCH signalling are associated with junctional destabilisation in neighbouring cells.

To confirm this observation, we evaluated the effect of VEGF in each cell type since, as shown before, VEGF increases average STB_Index in all cells (Figure 5C). As shown in Supplementary Figure 8B, we found that VEGF induced a significant reduction in the

frequency of NOTCH Low cells in HAoEC and HUVEC, this was accompanied by an increase in NOTCH High cells suggesting lateral inhibition mechanisms. Consistently, junctional stabilisation was less pronounced in HAoEC which have a high frequency of high cells at baseline therefore lateral inhibition could be dampened by excess and continuous NOTCH signalling in neighbouring cells.

These data demonstrate that VEGF treatment can modulate NOTCH signalling in HAoEC and HUVEC with similar effects of promoting junctional stabilisation but to different extents depending on initial conditions.

Finally, to verify that junctional stabilisation is associated with acquisition of overall quiescent EC phenotype we calculated the correlation between field averaged frequency of quiescent and stressed cells and junction stability index. Our results overall demonstrate a positive correlation between junction stability index and the frequency of quiescent cells and a negative correlation between the index and the frequency of stressed (migratory) cells in line with previous literature (Figure 7B).

Taken together, our data demonstrate that chronic supra-physiologic VEGF induces junction stabilisation in HAoEC and HUVEC via increase of NOTCH signalling coupled with lateral inhibition in neighbouring cells and that this effect is dependent from initial conditions (intrinsic NOCTH signalling). This effect is mediated by selective reduction of Low NOTCH signalling EC and therefore, by demonstrating that heterogeneity in NOTCH activation produces physiologically relevant and distinct phenotypes our data also provide a clear experimental evidence that EC metastability within the same monolayer is functionally relevant. Finally, chronic VEGF stimulation didn't significantly affect overall pattern of NOTCH active/inactive cells demonstrating that metastability of NOTCH signalling in EC monolayers is robust to chronic and supra-physiologic perturbation.

Discussion

EC exert a surprising variety of specialised functions[3,6] some of which are limited to specific organs while others are common, and this variety of functions is reflected in EC phenotypical heterogeneity. EC heterogeneity across different organs is explained by the activation of differential genetic programs (e.g., arterial, venous, capillary and lymphatic EC)[20,45]. This EC diversity arises during development, is preserved throughout homeostasis and is thought to be led by micro environmental factors. Heterogeneity within the same vascular bed where microenvironmental factors are stable (or undergoing minor fluctuations) has been observed[17] and deemed crucial to understand variable functions within the same EC type. Strategies such as Hedge Betting (where heterogeneity expands the repertoire of possible responses) or Swarm Sensing (where pioneer cells can redirect the response of neighbouring cells in a cascade) are thought to be employed by homogeneous cells population to expand the repertoire of sensory and adaptative responses[11].

These mechanisms require similar cells to preserve discrete, different and adaptable phenotypes and the time scale at which these phenotypes change (minutes) is much smaller than that of gene expression (hours). Thus, to justify rapid phenotype switches it is necessary to involve inherently dynamic processes such as junctional plasticity.

Direct evaluation of dynamic changes in cell connectivity, functions and phenotype ideally requires observing live cells at a timescale compatible with that of the phenomena under investigation and this poses considerable technical hurdles. Therefore, despite great advances in live-microscopy, comprehensive cell phenotyping of single cells at population level is still vastly relying on fixed immuno-stained cells. Although, observation of end-point cells cannot provide information on the exact dynamics of the system, extensive profiling of single cells can inform about cell dynamic behaviours and help to develop hypotheses which can be demonstrated experimentally or with mathematical models and computational methods[38].

Aiming to grasp a better understanding of endothelial cells' heterogeneity, connectivity and emerging dynamic behaviours[16,17] we developed ECPT and characterised three EC lines

385 under standard conditions or supra-physiological (like those observed in cancer) levels of
386 VEGF. In line with previously published data[20] our data demonstrate that Human Aortic,
387 Umbilical Vein or Pulmonary EC present clearly distinct phenotypes (Figure 2-6), maintained
388 at steady state, independently from microenvironmental stimuli. The three cell types have
389 distinct intrinsic proliferative potential and demonstrate diffuse ability to proliferate, in contrast
390 to the idea that EC undergo terminal differentiation and lose proliferative capacity[7].
391 Our findings are consistent with a model of monolayer maintenance hosting intermediate EC
392 populations with different proliferation potential. This effect could be achieved by a stem-
393 precursor-differentiated hierarchy as proposed by Patel et al.[21], or by an alternative model
394 positing proliferating EC and quiescent EC as in metastable states (Figure 2-3 and
395 Supplementary Figure 12). Thus, single EC could undergo a temporary reversion of the
396 differentiation programme in response to specific conditions, generate an adequate progeny
397 and return to quiescence (Supplementary Figure 12)[39]. Such state would eliminate the need
398 for a defined intermediate EC phenotype and would be more efficient at repairing localised
399 endothelial damage. Our data support this latter concept as we found a significant fraction of
400 proliferating EC far from closely packed and highly proliferative colonies (Figure 3) and is also
401 supported by EC monolayer scratch assays where most cells at the edge of the scratch
402 promptly activate, migrate and start proliferating until confluence is reached (not shown)[40] and
403 by many evidences that EC proliferation is contact inhibited and chiefly regulated by
404 decreased EC connectivity and lateral inhibition (during angiogenesis)[41,42], implicating that the
405 default EC state might be proliferation not quiescence and that in turn quiescence should be
406 achieved actively[39]. Under our experimental conditions, both HUVEC and HAoEC had a
407 similar sustained proliferative potential (on average >10% cells in cell cycle for each
408 microscopic field) and as expected VEGF induced increased proliferation in all EC examined.
409 The observed induction was small (~1% in all cells) as under our experimental conditions EC
410 are confluent and thus largely contact inhibited. Nonetheless ongoing sustained proliferation
411 in a confluent monolayer suggest that EC might require additional stimuli (some of which might
412 be absent *in vitro*) to further inhibit proliferation. Overall, our data on proliferation support a
413 model where EC can enter cell cycle at need notwithstanding opposing signalling including
414 EC-EC contact. We also demonstrate that clusters of fast proliferating EC existed within
415 confluent monolayers and under our experimental conditions (confluent EC) is highly unlikely
416 that enough space is created to allow more than one/two cell divisions before insurgence of
417 contact inhibition. Therefore, these observations are consistent with the existence of highly
418 clonogenic EC sparsely scattered throughout the monolayer. It remains to be elucidated
419 whether these colony forming EC are a distinct subpopulation (i.e., a true EC precursor driven
420 by a specific transcriptional programme) or the result of stochastic fluctuations in expression
421 of genes related to cell cycle. In this sense, the Rafii laboratory[43] has recently demonstrated
422 that exogenous overexpression of ETV2 in primary EC reprogrammes cells toward a highly
423 clonogenic phenotype. Therefore, reactivation of ETV2 might be a potential physiologic
424 mechanism to rejuvenate EC pools by creating new EC precursors but evidences of this
425 occurring in physiologic conditions in vivo has not been reported so far and warrants further
426 investigations.

427 Inter-endothelial junctions (IEJ) are among the main drivers of EC biology mediating high-level
428 functions such as endothelial barrier permeability and leukocyte trafficking and low-level
429 functions such as contact inhibition of proliferation. Analysis of IEJ in three different EC
430 populations highlighted a high degree of junctional heterogeneity in HAoEC and HUVEC, while
431 HPMEC junctions where homogeneously stable. Here, we adopted the "stabilised"
432 nomenclature as these junctions are structurally more complex and wider than linear ones
433 which we interpreted as areas where EC membranes overlap forming a junctional plate
434 (Figure 5A). The amount of membrane engaged in the junction is associated with higher
435 junction strength since a larger area will correspond to more intercellular VEC-VEC

interactions which in turn are responsible for maintenance of adhesion[44]. Inter-endothelial connectivity is also a regulator of contact-dependent signalling pathways. In line with previous literature, we show that HAoEC (arterial) had more linear (stabilised) junctions than HUVEC (venous) which instead tended to form highly dynamic jagged junctions. IEJ chiefly regulate traffic of molecules and solutes in and out of capillaries and inhibit coagulation by preventing exposure of underlying sub-intimal layer in arteries and veins. Importantly, HPMEC had stabilised junctions and HAoEC had mostly linear junctions and presented stress fibres. This is reminiscent of the unique role of the pulmonary and arterial vessels in tightly regulate solute exchange or adapt to high flow respectively.

Distinctive features among different EC populations seem to be hard coded within cell gene expression program as cells from individual donors had vastly overlapping phenotypes and the features where maintained in all lines upon several passages in culture. Nonetheless, analysis of single cell data highlighted extensive heterogeneity within the same population. If decision whether to enter cell cycle or to maintain stable junction were dependent on differential gene expression, we would expect to find a limited collection of homogeneous phenotypes whereas we find an apparently continuous nuance of EC phenotypes within the same EC monolayer. Furthermore, it is established that these decisions need to be taken at a faster pace than gene expression could justify[17].

As mentioned, rapid phenotype switch between the same cell population is justified by involving dynamic genetic circuits dominated by oscillatory or stochastic behaviours[10]. We focussed our attention on NOTCH signalling as its role in EC biology and its crosstalk with the junctional complex is well recognised[37]. Furthermore, NOTCH has been proposed as a master switch which dynamics can deploy either mono-stable, bi-stable or metastable cell states[42]. In the context of angiogenesis, it has been demonstrated that leading tip cells induce NOTCH signalling in trailing stalk cells via Dll4-NOTCH1 leading to lateral inhibition of the tip cell phenotype[42] whereas EC within a stabilised monolayer cannot acquire a tip cell phenotype and all EC within a monolayer receive in principle similar NOTCH stimulation from neighbours. Three scenarios could thus arise 1) mono-stable, where most non dividing cells accumulate NICD to a characteristic carrying capacity proportional to basal expression levels of NOTCH agonists such as Dll4 (e.g., high in arteries and low/absent in vein), 2) bi-stable, where cells oscillate between ON and OFF states due to lateral inhibition/induction until they ultimately settle on one of the two and 3) non-stable/metastable, where cells do not settle on specific states and instead constantly oscillate generating in the process differential levels of signalling. In a mono-stable scenario cells will favour a specific phenotype until perturbation occurs. In a bi-stable scenario ON and OFF cells will tend to acquire characteristic distributions or patterns (e.g., boundaries). Metastability is more flexible as the acquisition of phenotype can depend on both the overall intensity of the original signal and the frequency at which this oscillates, and this favour the emergence of biological noise and stochastic behaviours which in principle can deploy a much higher degree of variability[17].
EC monolayers have been previously described as either NOTCH active or inactive especially in the context of arteriovenous specification[45] and downstream NOTCH genes are often used as surrogate markers of the arterial phenotype[46]. Fluctuations in NOTCH signalling have been hypothesised in EC monolayers and demonstrated in EC during sprouting angiogenesis[42]. NOTCH signalling has been linked to both inhibition of EC proliferation[47] and increased junction stabilisations[37] but NOTCH regulation in EC monolayer at the single cell resolution has not been investigated previously.
By measuring NICD in a relatively large collection of single cell measurements, we found that different EC within their monolayer acquire metastable NOTCH activation states which can be modulated by chronic VEGF treatment and are used to regulate overall junctional stability of the monolayer. Since NOTCH signalling is titratable[48] different extent of signalling could generate different phenotypes with ON state. Therefore, our data provide a first demonstration of recent hypotheses[16,17] where heterogeneity and metastability were postulated as relevant

489 mechanism for swarm sensing behaviours in EC monolayers and as underlying mechanisms
490 for EC phenotypical plasticity and adaptability.
491 We also show for the first time that microvascular EC can possess high levels of NOTCH
492 activity as demonstrated by our data on HPMEC, which cannot be explained by the currently
493 established model positing high NOTCH activity as a mediator of arterial phenotype. In other
494 words, despite sustained NOTCH signalling is a hallmark of arterial cells it cannot be
495 accounted as the sole or main pathway involved in the establishment of the arterial phenotype
496 warranting revision of protocols to generate stem cells derived arterial or venous EC[32].
497 NOTCH signalling in HPMEC wasn't affected by VEGF (Supplementary Figure 8 B) possibly
498 because the frequencies of NOTCH Low and NOTCH High cells were already the highest and
499 lowest respectively (within our experiments) at baseline and these levels might represent set
500 boundaries of possible VEGF modulation. Overall, our results regarding VEGF-mediated
501 NOTCH modulation in different EC lines strongly support the idea that the net effects of chronic
502 VEGF stimulation are sensibly dependent from initial conditions (i.e., the intrinsic baseline
503 NOTCH signalling levels) and might lead to appreciably different responses in different EC.
504
505 Altogether, our data provide the first direct evidence that metastable cell states orchestrate
506 the stability and plasticity of EC monolayers, and that EC within monolayers use NOTCH and
507 junction's machinery to constantly probe their neighbourhood relaying spatial and relational
508 information to the gene expression machinery and deploying different phenotypes in a
509 localised and context dependent manner. We suggest that phenotypical diversity within a
510 homogeneous EC population can represent a cellular implementation of "Bet hedging",
511 "Swarm sensing" or "Response distribution" mechanisms[15] to deploy a globally stable but
512 locally adaptable tissue such as the endothelium.
513
514 Our in vitro approach allows focussing on intrinsic EC mechanisms of monolayer maintenance
515 and plasticity excluding variability caused by microenvironmental factors and it has been
516 highlighted that the heterogeneity of different blood vessels found in vivo is sustained by EC
517 rather than perivascular cells heterogeneity[18]. Therefore, it seems highly probable that the
518 robust metastability in EC phenotypes described above has a direct relevance to more
519 complex in vivo context. It will be important to elucidate in future studies how the crosstalk
520 with perivascular cells and microenvironment can affect emerging endothelial behaviours.
521
522 These results imply that pharmacological interventions targeting the endothelium need to
523 account for dynamic adaptive mechanisms which might otherwise unpredictably dampen or
524 exacerbate the efficacy of EC targeting drugs (e.g., VEGF or VEGF receptors inhibitors).
525 Otherwise, adaptive mechanisms might be exploited to precisely targeting EC subsets of
526 interest while leaving most of the other EC un-perturbed.
527
528 In conclusion, we have built on our previous work to create ECPT, a powerful platform to
529 dissect single cell level phenotypical composition of EC monolayers enabling for the first time
530 to demonstrate EC heterogeneity as a driving force of endothelial plasticity. We envisage that
531 coupling ECPT with live imaging setups and single cells transcriptomic analysis will open the
532 way to a much deeper understanding of emerging dynamic endothelial behaviours and thus
533 to develop novel more effective therapies for prevention of cardiovascular diseases and the
534 treatment of cancer.
535
536
537 **Methods**
538
539 Cell culture
540 HUVEC, HAoEC and HDMEC (PromoCell) were plated on 10 µg/mL fibronectin (from human
541 plasma, Promocell)-coated flasks, grown in EGMV2 medium (Promocell) in the absence of
542 antibiotics, detached with Accutase (Thermo Fisher Scientific, Waltham, MA), and used by
543 passage 5. For experiments, 4×10^4 ECs per well were seeded in fibronectin-coated 96-well

544 plates (µclear, Greiner) and cultured for 48 h under basal (EGMV2, Promocell) or activated
545 (EGMV2 + 50 ng/mL VEGFA, Peprotech, London, UK) conditions in triplicate. The ECs formed
546 confluent monolayers at the time of immunostaining and image acquisition.
547
548 Immunostaining
549 Cells were fixed with 2% paraformaldehyde in phosphate buffered saline (PBS) for 10 minutes
550 at room temperature. Cells were blocked 1h with PBS supplemented with 1% fetal bovine
551 serum (FBS) and permeabilised with 0.1% Triton X 100. Cells were then incubated for 1h at
552 room temperature with primary antibodies against CDH5 (Ve-Cadherin Novusbio NB600-
553 1409, 1 µg/mL final) and activated NOTCH (NICD, Abcam ab8925, 1 µg/mL final). CDH5 is a
554 lineage marker for EC and cells were all CDH5+, the anti-activated NOTCH1 reveals NOTCH
555 intracellular domain (NICD) puncta. Plates were washed and incubated 1h with 1 µg/mL
556 secondary Alexa 488-conjugated antibody and Alexa-555-conjugated antibody (Thermo),
557 Hoechst 33342 (1 µg/mL, Sigma) and Phalloidin-Atto 647N (Sigma).
558
559 Image Acquisition
560 We obtained images from slides with an Operetta CLS system (PerkinElmer, Waltham, MA)
561 equipped with a 40×water-immersion lens (NA 1.1). In each well, 3 areas were acquired. Each
562 area is composed of nine microscopic fields at 40× magnification (Supplementary Figure 1).
563 We standardised acquisition parameters (led power, exposure time) throughout different
564 experiments and used HUVEC as a standard for calibration in all experiments. We analysed
565 an image database containing 6028 images (1507 fields in four fluorescence channels)
566 extracted from four independent experiments conducted on EC lines from two different donor
567 each. Three intraexperiment replicates were conducted for each experiment.
568
569
570 Endothelial Cell Profiling Tool
571 We used a combination of machine learning-aided image segmentation (ImageJ)[49] and an
572 image-based cell profiling tool (CellProfiler)[50] to extract the phenotype of single EC in
573 monolayers. Our workflow enables to measure EC morphology (Area, perimeter, shape
574 descriptors, cell neighbours), NICD, VE-Cadherin and DNA intensities and to characterise
575 inter-endothelial junctions (IEJ). In the present study, we chose to analyse only selected
576 features with recognised functions in EC biology. Image texture features were measured and
577 only used during the training of machine learning algorithm[51,52] which in turn were used to
578 classify cell activation states and junction morphology. ECPT scripts and methods are detailed
579 in Appendix 1 and available at https://github.com/exr98/HCA-uncovers-metastable-
580 phenotypes-in-hEC-monolayers
581
582 We Imported and cleaned the results into R studio excluding artifacts and mis-segmented cell
583 objects. We then calculated derived continuous (Junctional stability index) and categorical
584 (Cell Cycle and NOCTH activation) parameters (Supplementary Table 1). Following guidelines
585 suggested by Caceido et al.[53] We pre-processed the database to exclude miss-segmented
586 cells and to normalise the measurements prior to dimensionality reduction or single factor
587 analysis. Our final dataset was composed of measurements of 29 parameters from 104416
588 single cells (Supplementary Table 1)
589 We conducted PCA analysis on cluster of ECPT parameters (Cell morphology, intensity,
590 neighbourhood and junctional status, Supplementary Table 1) and generated 12 PCA
591 components which we fed into the tSNE algorithm.
592 We performed tSNE using different perplexity values (5, 10, 20, 40, 60, 80) and ran the
593 algorithm with 1000 iterations, all tSNE plots displayed correspond to 10 perplexity.
594
595 We created a shiny application for interactive selection of data of interest from t-SNE
596 scatterplots (Appendix 1). This application[54] allowed specific cluster analysis by subclustering
597 and further analysis in the R environment[55]. All files containing the code required to reproduce

the shiny application using our dataset are available on https://github.com/exr98/HCA-uncovers-metastable-phenotypes-in-hEC-monolayers.

Statistical analysis

To compare multiple groups, we used one-way ANOVA followed by Tuckey's HSD post-hoc test. We considered $p < 0.05$ (*) significative and $p<0.01$ (**), $p<0.001$ (***) and $p<0.0001$(****) highly significative. To evaluate linear correlation between continuous variables we calculated Pearson's Correlation coefficient (*R*) and considered $p<0.001$ as highly statistically significative.

References

1- Potente, M., Gerhardt, H. and Carmeliet, P., 2011. Basic and Therapeutic Aspects of Angiogenesis. *Cell*, 146(6), pp.873-887.

2- Park-Windhol, C. and D'Amore, P., 2016. Disorders of Vascular Permeability. *Annual Review of Pathology: Mechanisms of Disease*, 11(1), pp.251-281.

3- Augustin, H. and Koh, G., 2017. Organotypic vasculature: From descriptive heterogeneity to functional pathophysiology. *Science*, 357(6353), p.eaal2379.

4- Kusumbe, A., Ramasamy, S. and Adams, R., 2014. Coupling of angiogenesis and osteogenesis by a specific vessel subtype in bone. *Nature*, 507(7492), pp.323-328.

5- Itkin, T., Gur-Cohen, S., Spencer, J., Schajnovitz, A., Ramasamy, S., Kusumbe, A., Ledergor, G., Jung, Y., Milo, I., Poulos, M., Kalinkovich, A., Ludin, A., Golan, K., Khatib, E., Kumari, A., Kollet, O., Shakhar, G., Butler, J., Rafii, S., Adams, R., Scadden, D., Lin, C. and Lapidot, T., 2016. Distinct bone marrow blood vessels differentially regulate haematopoiesis. *Nature*, 532(7599), pp.323-328.

6- Rafii, S., Butler, J. and Ding, B., 2016. Angiocrine functions of organ-specific endothelial cells. *Nature*, 529(7586), pp.316-325.

7- Yoder, M., 2017. Endothelial stem and progenitor cells (stem cells): (2017 Grover Conference Series). *Pulmonary Circulation*, 8(1), p.204589321774395.

8- Greco Song, H., Rumma, R., Ozaki, C., Edelman, E. and Chen, C., 2018. Vascular Tissue Engineering: Progress, Challenges, and Clinical Promise. *Cell Stem Cell*, 22(4), p.608.

9- Siu, D., Lee, K., Lo, M., Stassen, S., Wang, M., Zhang, I., So, H., Chan, G., Cheah, K., Wong, K., Hsin, M., Ho, J. and Tsia, K., 2020. Deep-learning-assisted biophysical imaging cytometry at massive throughput delineates cell population heterogeneity. *Lab on a Chip*, 20(20), pp.3696-3708

10- MacLean, A., Hong, T. and Nie, Q., 2018. Exploring intermediate cell states through the lens of single cells. *Current Opinion in Systems Biology*, 9, pp.32-41.

11- Dueck, H., Eberwine, J. and Kim, J., 2015. Variation is function: Are single cell differences functionally important? *BioEssays*, 38(2), pp.172-180.

12- Eling, N., Morgan, M. and Marioni, J., 2019. Challenges in measuring and understanding biological noise. *Nature Reviews Genetics*, 20(9), pp.536-548.

13- Kalucka, J., de Rooij, L., Goveia, J., Rohlenova, K., Dumas, S., Meta, E., Conchinha, N., Taverna, F., Teuwen, L., Veys, K., García-Caballero, M., Khan, S., Geldhof, V., Sokol, L., Chen, R., Treps, L., Borri, M., de Zeeuw, P., Dubois, C., Karakach, T., Falkenberg, K., Parys, M., Yin, X., Vinckier, S., Du, Y., Fenton, R., Schoonjans, L., Dewerchin, M., Eelen, G., Thienpont, B., Lin, L., Bolund, L., Li, X., Luo, Y. and Carmeliet, P., 2020. Single-Cell Transcriptome Atlas of Murine Endothelial Cells. *Cell*, 180(4), pp.764-779.e20.

14- Tikhonova, A., Dolgalev, I., Hu, H., Sivaraj, K., Hoxha, E., Cuesta-Domínguez, Á., Pinho, S., Akhmetzyanova, I., Gao, J., Witkowski, M., Guillamot, M., Gutkin, M., Zhang, Y., Marier, C., Diefenbach, C., Kousteni, S., Heguy, A., Zhong, H., Fooksman, D., Butler, J., Economides, A., Frenette, P., Adams, R., Satija, R., Tsirigos, A. and Aifantis, I., 2019. The bone marrow microenvironment at single-cell resolution. *Nature*, 569(7755), pp.222-228.

15- Acar, M., Mettetal, J. and van Oudenaarden, A., 2008. Stochastic switching as a survival strategy in fluctuating environments. *Nature Genetics*, 40(4), pp.471-475.

16- McCarron, J., Lee, M. and Wilson, C., 2017. The Endothelium Solves Problems That Endothelial Cells Do Not Know Exist. *Trends in Pharmacological Sciences*, 38(4), pp.322-338.

17- McCarron, J., Wilson, C., Heathcote, H., Zhang, X., Buckley, C. and Lee, M., 2019. Heterogeneity and emergent behaviour in the vascular endothelium. *Current Opinion in Pharmacology*, 45, pp.23-32.

18- Chavkin, N. and Hirschi, K., 2020. Single Cell Analysis in Vascular Biology. *Frontiers in Cardiovascular Medicine*, 7.

19- Wiseman, E., Zamuner, A., Tang, Z., Rogers, J., Munir, S., Di Silvio, L., Danovi, D. and Veschini, L., 2019. Integrated Multiparametric High-Content Profiling of Endothelial Cells. *SLAS DISCOVERY: Advancing the Science of Drug Discovery*, 24(3), pp.264-273.

20- Chi, J., Chang, H., Haraldsen, G., Jahnsen, F., Troyanskaya, O., Chang, D., Wang, Z., Rockson, S., van de Rijn, M., Botstein, D. and Brown, P., 2003. Endothelial cell diversity revealed by global expression profiling. *Proceedings of the National Academy of Sciences*, 100(19), pp.10623-10628.

21- Patel, J., Seppanen, E., Rodero, M., Wong, H., Donovan, P., Neufeld, Z., Fisk, N., Francois, M. and Khosrotehrani, K., 2017. Functional Definition of Progenitors Versus Mature Endothelial Cells Reveals Key SoxF-Dependent Differentiation Process. *Circulation*, 135(8), pp.786-805.

22- Vigilante, A., Laddach, A., Moens, N., Meleckyte, R., Leha, A., Ghahramani, A., Culley, O., Kathuria, A., Hurling, C., Vickers, A., Wiseman, E., Tewary, M., Zandstra, P., Durbin, R., Fraternali, F., Stegle, O., Birney, E., Luscombe, N., Danovi, D. and Watt, F., 2019. Identifying Extrinsic versus Intrinsic Drivers of Variation in Cell Behavior in Human iPSC Lines from Healthy Donors. *Cell Reports*, 26(8), pp.2078-2087.e3.

23- Millán, J., Cain, R., Reglero-Real, N., Bigarella, C., Marcos-Ramiro, B., Fernández-Martín, L., Correas, I. and Ridley, A., 2010. Adherens junctions connect stress fibres between adjacent endothelial cells. *BMC Biology*, 8(1).

24- Veschini, L., Crippa, L., Dondossola, E., Doglioni, C., Corti, A. and Ferrero, E., 2011. The vasostatin-1 fragment of chromogranin A preserves a quiescent phenotype in hypoxia-driven endothelial cells and regulates tumor neovascularization. *The FASEB Journal*, 25(11), pp.3906-3914.

25- Roukos, V., Pegoraro, G., Voss, T. and Misteli, T., 2015. Cell cycle staging of individual cells by fluorescence microscopy. *Nature Protocols*, 10(2), pp.334-348

26- Fernández-Martín, L., Marcos-Ramiro, B., Bigarella, C., Graupera, M., Cain, R., Reglero-Real, N., Jiménez, A., Cernuda-Morollón, E., Correas, I., Cox, S., Ridley, A. and Millán, J., 2012. Crosstalk Between Reticular Adherens Junctions and Platelet Endothelial Cell Adhesion Molecule-1 Regulates Endothelial Barrier Function. *Arteriosclerosis, Thrombosis, and Vascular Biology*, 32(8).

27- Veschini, L., Belloni, D., Foglieni, C., Cangi, M., Ferrarini, M., Caligaris-Cappio, F. and Ferrero, E., 2006. Hypoxia-inducible transcription factor–1 alpha determines sensitivity of endothelial cells to the proteosome inhibitor bortezomib. *Blood*, 109(6), pp.2565-2570.

28- Ferrero, E., Scabini, S., Magni, E., Foglieni, C., Belloni, D., Colombo, B., Curnis, F., Villa, A., Ferrero, M. and Corti, A., 2004. Chromogranin A protects vessels against tumor necrosis factor α-induced vascular leakage. *The FASEB Journal*, 18(3), pp.554-556.

29- Brezovjakova, H., Tomlinson, C., Mohd Naim, N., Swiatlowska, P., Erasmus, J., Huveneers, S., Gorelik, J., Bruche, S. and Braga, V., 2019. Junction Mapper is a novel computer vision tool to decipher cell–cell contact phenotypes. *eLife*, 8.

30- Seebach, J., Taha, A., Lenk, J., Lindemann, N., Jiang, X., Brinkmann, K., Bogdan, S. and Schnittler, H., 2015. The CellBorderTracker, a novel tool to quantitatively analyze spatiotemporal endothelial junction dynamics at the subcellular level. *Histochemistry and Cell Biology*, 144(6), pp.517-532.

31- Aranguren, X., Beerens, M., Coppiello, G., Wiese, C., Vandersmissen, I., Lo Nigro, A., Verfaillie, C., Gessler, M. and Luttun, A., 2013. COUP-TFII orchestrates venous and lymphatic endothelial identity by homo- or hetero-dimerisation with PROX1. *Journal of Cell Science*, 126(5), pp.1164-1175.

32- Zhang, J., Chu, L., Hou, Z., Schwartz, M., Hacker, T., Vickerman, V., Swanson, S., Leng, N., Nguyen, B., Elwell, A., Bolin, J., Brown, M., Stewart, R., Burlingham, W., Murphy, W. and Thomson, J., 2017. Functional

728 characterization of human pluripotent stem cell-derived arterial endothelial cells. *Proceedings of the National*
729 *Academy of Sciences*, 114(30), pp.E6072-E6078.
730
731 33- Zong, D., Li, J., Cai, S., He, S., Liu, Q., Jiang, J., Chen, S., Long, Y., Chen, Y., Chen, P. and Ouyang, R., 2018.
732 Notch1 regulates endothelial apoptosis via the ERK pathway in chronic obstructive pulmonary disease. *American*
733 *Journal of Physiology-Cell Physiology*, 315(3), pp.C330-C340.
734
735 34- Falo-Sanjuan, J. and Bray, S., 2019. Decoding the NOTCH signal. *Development, Growth & Differentiation*,
736 62(1), pp.4-14.
737
738 35- Agrawal, S., Archer, C. and Schaffer, D., 2009. Computational Models of the NOTCH Network Elucidate
739 Mechanisms of Context-dependent Signaling. *PLoS Computational Biology*, 5(5), p.e1000390.
740
741 36- Vujovic, F., Hunter, N. and Farahani, R., 2019. NOTCH pathway: a bistable inducer of biological noise?. *Cell*
742 *Communication and Signaling*, 17(1).
743
744 37- Bentley, K., Franco, C., Philippides, A., Blanco, R., Dierkes, M., Gebala, V., Stanchi, F., Jones, M., Aspalter,
745 I., Cagna, G., Weström, S., Claesson-Welsh, L., Vestweber, D. and Gerhardt, H., 2014. The role of differential VE-
746 cadherin dynamics in cell rearrangement during angiogenesis. *Nature Cell Biology*, 16(4), pp.309-321.
747
748 38- Altschuler, S. and Wu, L., 2010. Cellular Heterogeneity: Do Differences Make a Difference?. *Cell*, 141(4),
749 pp.559-563.
750
751 39- Marescal, O. and Cheeseman, I., 2020. Cellular Mechanisms and Regulation of Quiescence. *Developmental*
752 *Cell*, 55(3), pp.259-271.
753
754 40- Yang, Y., Jamilpour, N., Yao, B., Dean, Z., Riahi, R. and Wong, P., 2016. Probing Leader Cells in Endothelial
755 Collective Migration by Plasma Lithography Geometric Confinement. *Scientific Reports*, 6(1).
756
757 41- Bocci, F., Onuchic, J. and Jolly, M., 2020. Understanding the Principles of Pattern Formation Driven by NOTCH
758 Signaling by Integrating Experiments and Theoretical Models. *Frontiers in Physiology*, 11.
759
760 42- Ubezio, B., Blanco, R., Geudens, I., Stanchi, F., Mathivet, T., Jones, M., Ragab, A., Bentley, K. and Gerhardt,
761 H., 2016. Synchronization of endothelial Dll4-NOTCH dynamics switch blood vessels from branching to
762 expansion. *eLife*, 5.
763
764 43- Palikuqi, B., Nguyen, D., Li, G., Schreiner, R., Pellegata, A., Liu, Y., Redmond, D., Geng, F., Lin, Y., Gómez-
765 Salinero, J., Yokoyama, M., Zumbo, P., Zhang, T., Kunar, B., Witherspoon, M., Han, T., Tedeschi, A., Scottoni, F.,
766 Lipkin, S., Dow, L., Elemento, O., Xiang, J., Shido, K., Spence, J., Zhou, Q., Schwartz, R., De Coppi, P., Rabbany,
767 S. and Rafii, S., 2020. Adaptable haemodynamic endothelial cells for organogenesis and tumorigenesis. *Nature*,
768 585(7825), pp.426-432.
769
770 44- Giannotta, M., Trani, M. and Dejana, E., 2013. VE-Cadherin and Endothelial Adherens Junctions: Active
771 Guardians of Vascular Integrity. *Developmental Cell*, 26(5), pp.441-454.
772
773 45- Adams, R. and Alitalo, K., 2007. Molecular regulation of angiogenesis and lymphangiogenesis. *Nature Reviews*
774 *Molecular Cell Biology*, 8(6), pp.464-478.
775
776 46- Mack, J. and Iruela-Arispe, M., 2018. NOTCH regulation of the endothelial cell phenotype. *Current Opinion in*
777 *Hematology*, 25(3), pp.212-218.
778
779 47- Fang, J., Coon, B., Gillis, N., Chen, Z., Qiu, J., Chittenden, T., Burt, J., Schwartz, M. and Hirschi, K., 2017.
780 Shear-induced NOTCH-Cx37-p27 axis arrests endothelial cell cycle to enable arterial specification. *Nature*
781 *Communications*, 8(1).
782
783 48- Henrique, D. and Schweisguth, F., 2019. Mechanisms of NOTCH signaling: a simple logic deployed in time
784 and space. *Development*, 146(3), p.dev172148.
785
786 49- Schindelin, J., Arganda-Carreras, I., Frise, E., Kaynig, V., Longair, M., Pietzsch, T., Preibisch, S., Rueden, C.,
787 Saalfeld, S., Schmid, B., Tinevez, J., White, D., Hartenstein, V., Eliceiri, K., Tomancak, P. and Cardona, A., 2012.
788 Fiji: an open-source platform for biological-image analysis. *Nature Methods*, 9(7), pp.676-682.

789

790 50- Carpenter AE, Jones TR, Lamprecht MR, Clarke C, Kang IH, Friman O, Guertin DA, Chang JH, Lindquist RA,
791 Moffat J, Golland P, Sabatini DM (2006) CellProfiler: image analysis software for identifying and quantifying cell
792 phenotypes. Genome Biology 7:R100.

51-Jones, T., Kang, I., Wheeler, D., Lindquist, R., Papallo, A., Sabatini, D., Golland, P. and Carpenter, A., 2008. CellProfiler Analyst: data exploration and analysis software for complex image-based screens. *BMC Bioinformatics*, 9(1), p.482.

52-Jones, T., Carpenter, A., Lamprecht, M., Moffat, J., Silver, S., Grenier, J., Castoreno, A., Eggert, U., Root, D., Golland, P. and Sabatini, D., 2009. Scoring diverse cellular morphologies in image-based screens with iterative feedback and machine learning. *Proceedings of the National Academy of Sciences*, 106(6), pp.1826-1831.

53- Caicedo, J., Cooper, S., He0igwer, F., Warchal, S., Qiu, P., Molnar, C., Vasilevich, A., Barry, J., Bansal, H., Kraus, O., Wawer, M., Paavolainen, L., Herrmann, M., Rohban, M., Hung, J., Hennig, H., Concannon, J., Smith, I., Clemons, P., Singh, S., Rees, P., Horvath, P., Linington, R. and Carpenter, A., 2017. Data-analysis strategies for image-based cell profiling. *Nature Methods*, 14(9), pp.849-863.

54- Winston Chang, Joe Cheng, JJ Allaire, Yihui Xie and Jonathan McPherson (2020). shiny: Web Application Framework for R. R package version 1.5.0. https://CRAN.R-project.org/package=shiny

55- R Core Team (2020). R: A language and environment for statistical computing. R Foundation for Statistical Computing, Vienna, Austria. URL https://www.R-project.org/

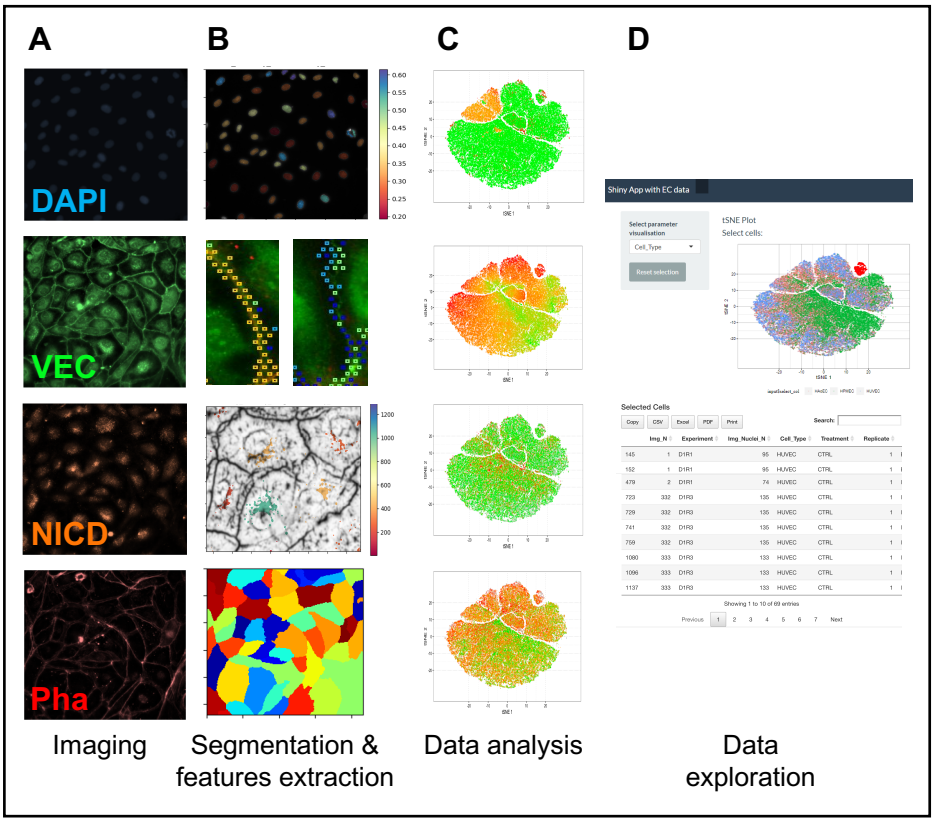

Figure 1 : ECPT workflow.
A) Acquisition of high resolution (40X OM) images on each channel (represented in false colours, original images are grey scale).
B) Features extraction and representation (ImageJ, Cell Profiler, Cell Profiler Analyst, R Studio).
C) tSNE plots of features normalised and grouped by biological function. Colouring in panels (Top to bottom) correspondent to Cell cycle, STB junctions, NOTCH Activation classes and Cell activation classes.
D) Shiny app (https://shiny.rstudio.com) enabling exploration of datasets, data extraction and iterative exploration.

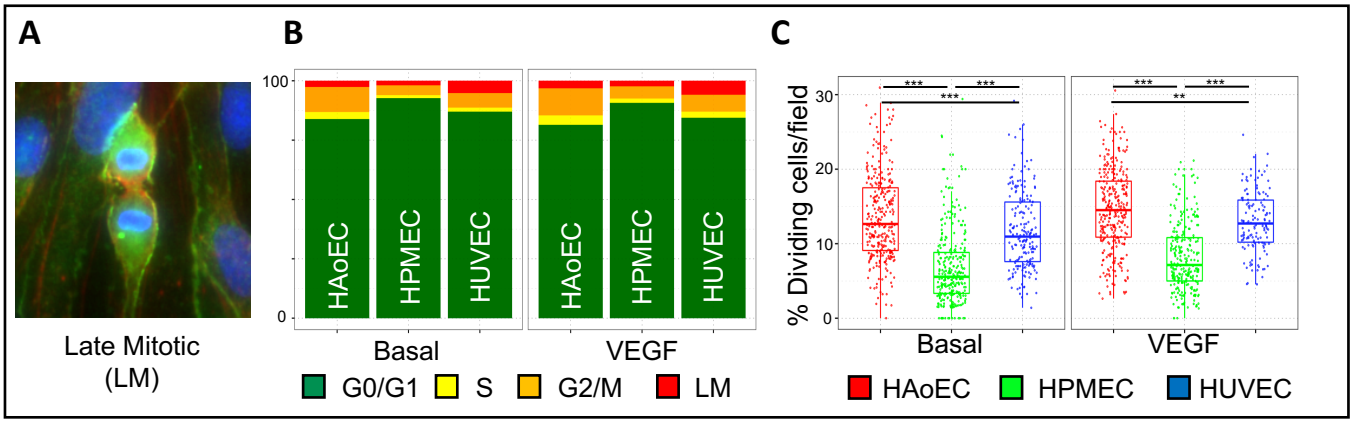

Figure 2: A) Late mitotic cells, LM. LM, were counted by AI aided cell classification (CPA, Fast gentle boosting). B) Cell cycle analysis of HUVEC, HAoEC and HPMEC in basal conditions or upon treatment with 50 ng/ml VEGF. C) Average of dividing (G2/M+S+LM) HUVEC, HAoEC and HPMEC per microscopic field in basal conditions or upon treatment with 50 ng/ml VEGF.

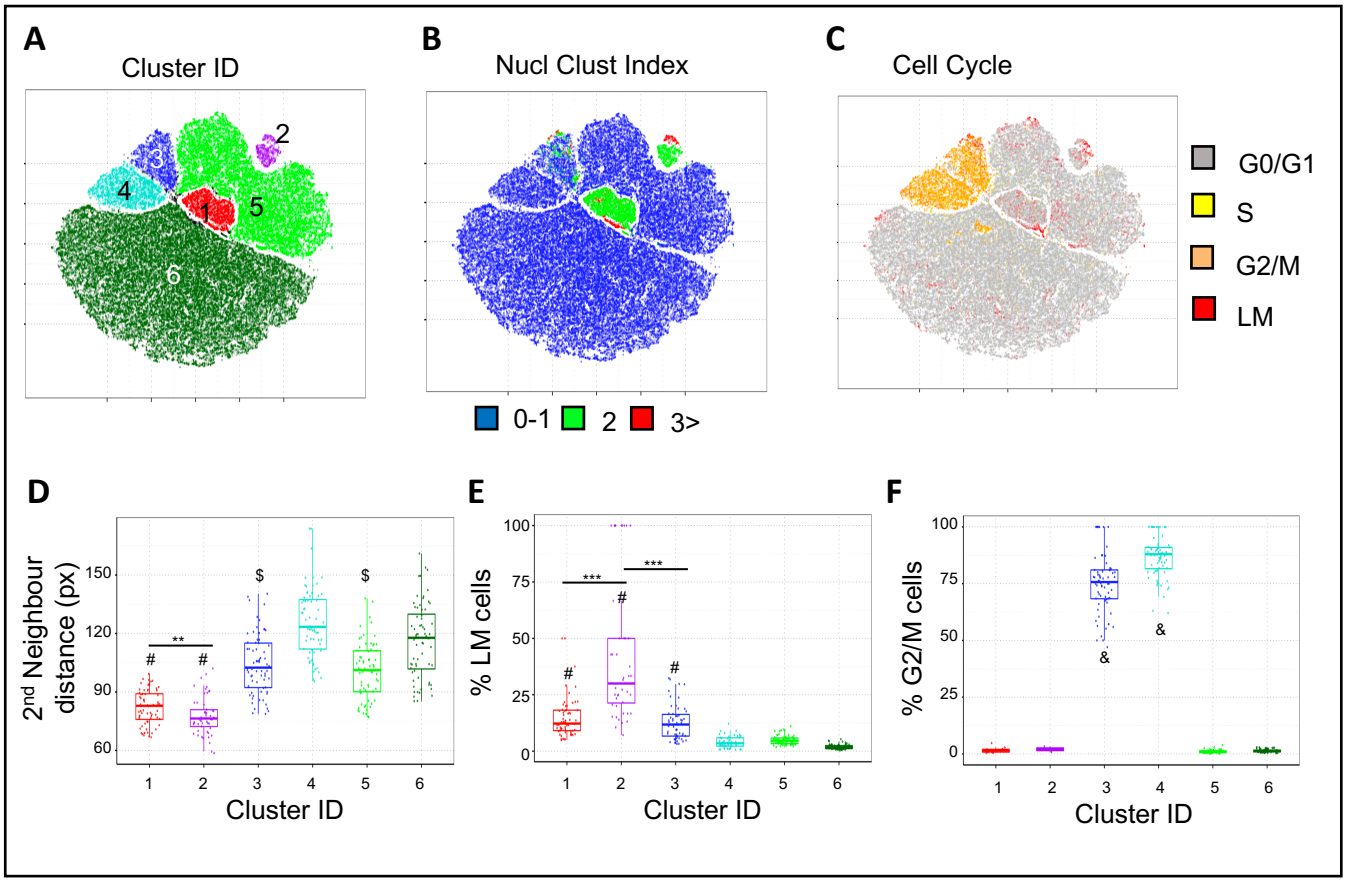

Figure 3: A) tSNE clusters mapped on tSNE scatterplot. B) Mapping of Nuclei Clustering Index in tSNE scatterplot. C) Mapping of Cell cycle categories in tSNE scatterplot. D) Average 2nd neighbour distance per well in the six clusters. E) Percent of late mitotic (LM) cells per well in the six clusters. F) Percent of G2/M cells per well in the six clusters. ** $p<0.001$, $ $p<0.0001$ against clusters 4 and 6, # $p<0.0001$ against clusters 4,5,6, & $p<0.0001$ against clusters 1,2,5,6.

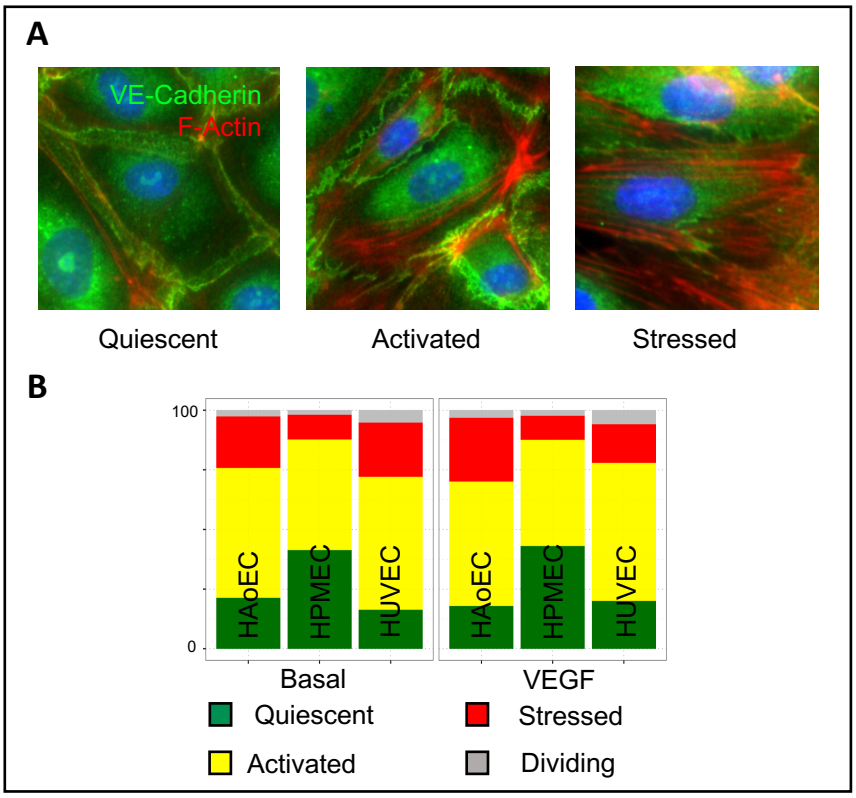

Figure 4: A) Examples of quiescent, activated and stressed EC. B) Cell activation classes in HUVEC, HAoEC and HPMEC in basal conditions or upon treatment with 50 ng/ml VEGF.

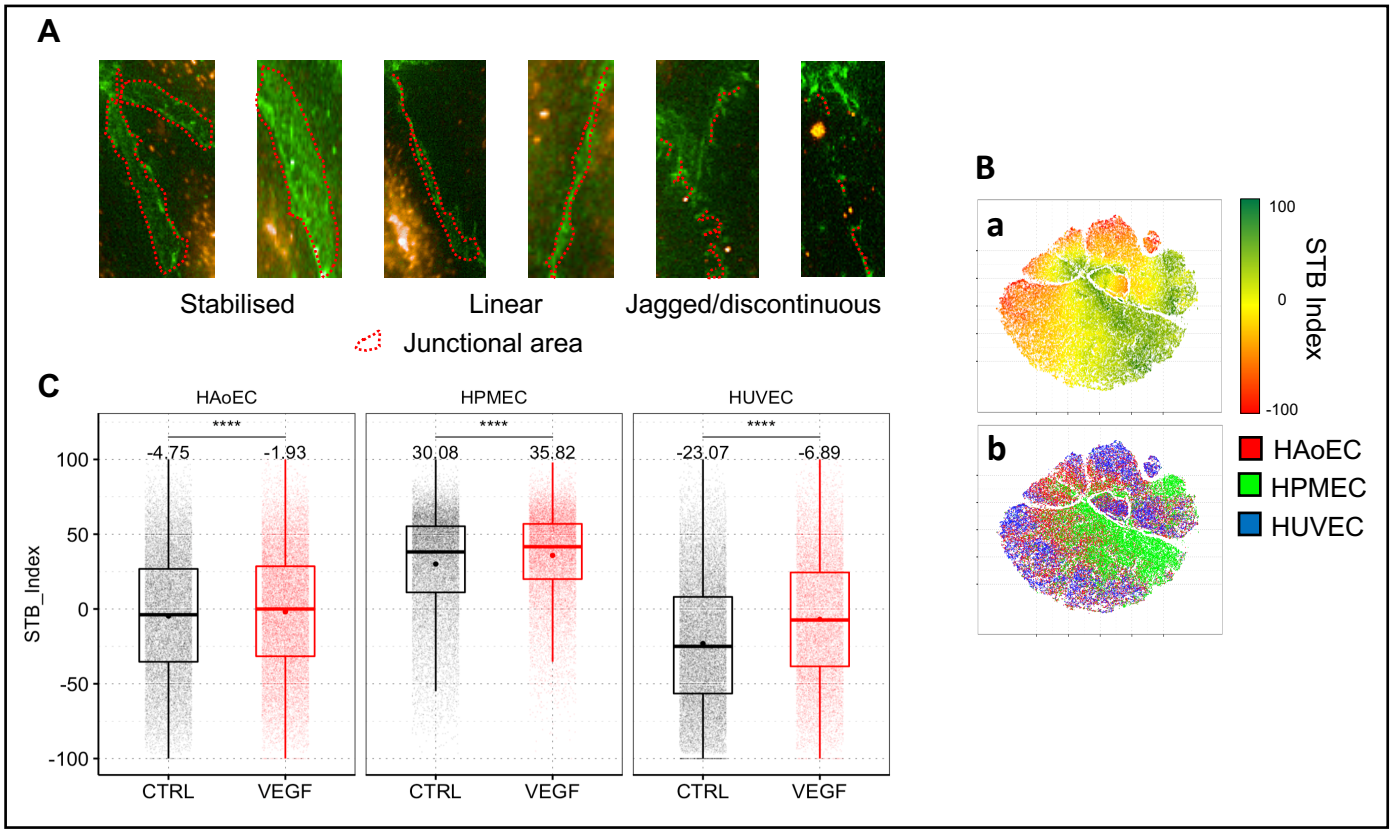

Figure 5: A) Examples of stabilised, linear and jagged or discontinuous junctions. B) Mapping of junctional stability index (a) and cell types (b) on tSNE scatterplot. C) Distribution of STB Index in HUVEC, HAoEC and HPMEC either under basal conditions (black) or 50ng/ml VEGF (red).

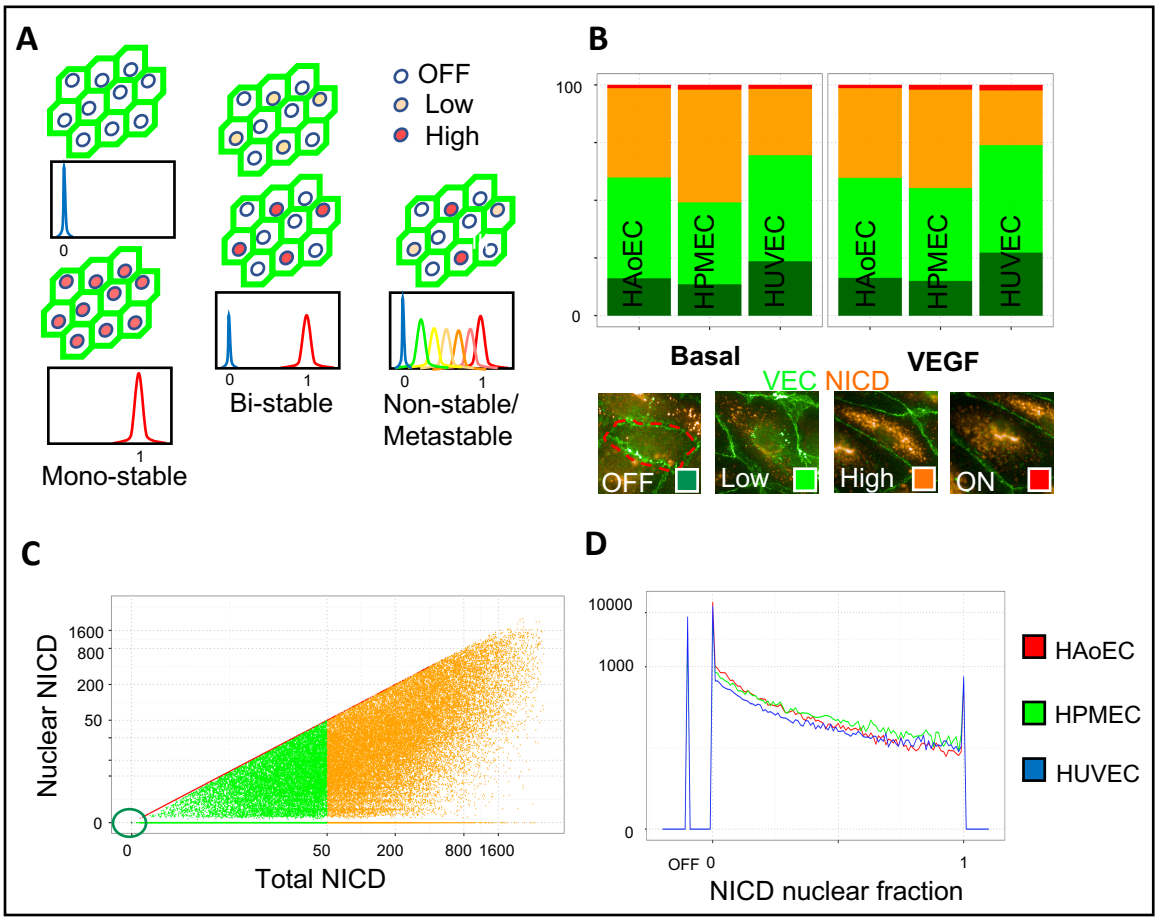

Figure 6:A) Schematic representing the possible configurations of notch activation at the population level. B) Distribution of NOTCH activation classes in HAoEC, HPMEC and HUVEC in basal conditions or upon treatment with 50 ng/ml VEGF C) Total vs Nuclear NICD intensity scatter plot. Cells without NICD are concentrated on the origin of the axes. Cells aligned along y axis (Nu Fraction =0) have varying degree of cytoplasmic NOTCH puncta and none in the nuclei. Cells on the diagonal (Nu fraction =1) have varying degrees of NOCTH puncta in the nuclei and none in the cytoplasm. Colours indicates the threshold used in the definition of categories in B, the threshold is set to 50 corresponding to 1-2 NOTCH puncta either in cytoplasm or nucleus. D) Density plot of Nuclear fraction of NICD intensity. The two peaks of NOTCH OFF and NOTCH ON (NICD Nu Fraction = 1) cells are evident. The majority of cells had intermediate activation states (NICD Nu Fraction >0 and < 1)

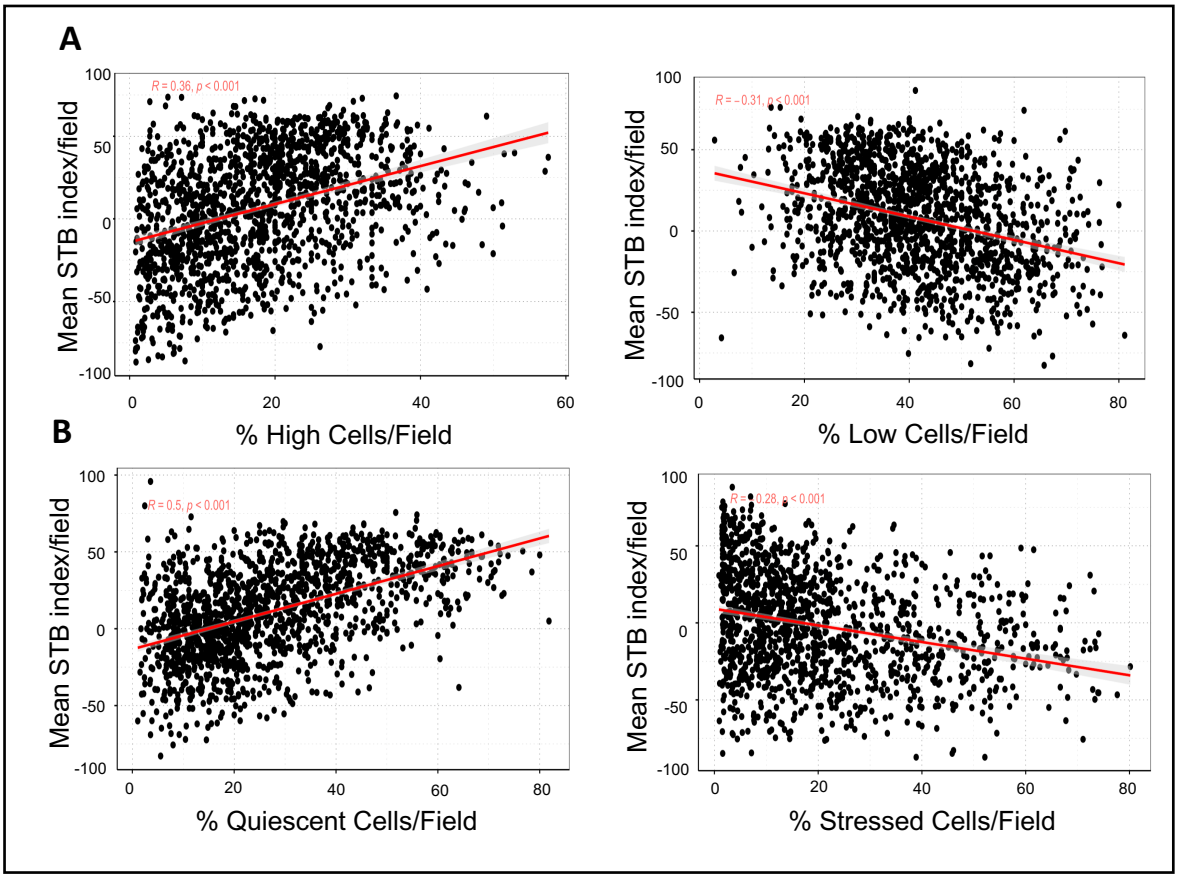

Figure 7: A) Field averaged measurements of Junctional stability index and percentage of NICD "Low" or "ON". Stability junction index positively correlated (R=0.43, P<0.001) with the frequency of ON cells and anticorrelated with the frequency of Low cells (R= -0.3, P<0.001). B) Field averaged measures of Junctional stability index and percentage of "quiescent" or "Stressed" cells.

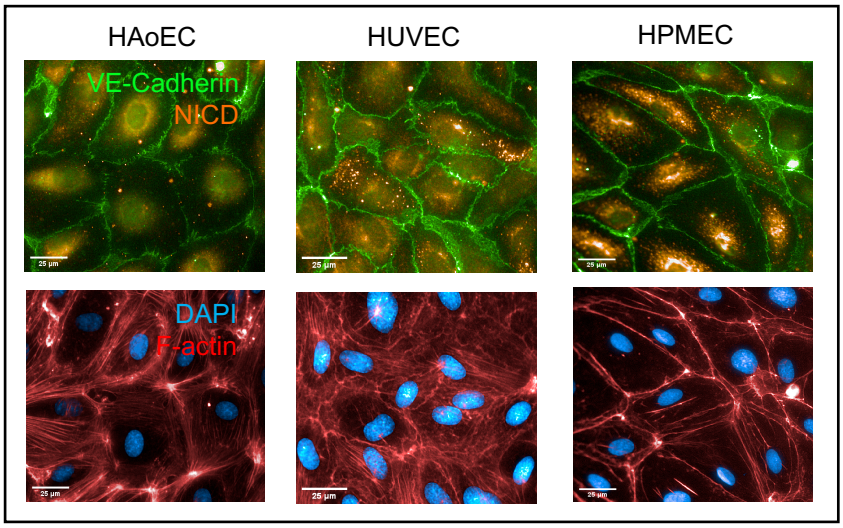

Supplementary Figure 1: Microphotographs comparing HUVECs, HAoEC and HPMEC untreated immunostained for VE-cadherin (green), NICD (orange), F-actin (red) and DAPI (blue); (scale bar: 25µm)

Original Parameters	PCAs	
Cell Metadata		
Cell Activation Class	A	
Cell Orientation		
Cell Area		
Cell Perimetre		
Cell Max Length		
Cell Min Length		
Widt/length Ratio		
Number of Neighbours	B	
Distance from closest Neighbour		
Distance from second closest Neighbour		
Nuclei Clustering Index		
Nuclei Distance from closest Neighbour		
Nuclei Distance from second closest Neighbour		
Nuclear Area		
DNA Intensity		D
Cell Cycle Class		
Cell CDH5 intensity		D
Junctional CDH5 Intensity		
CDH5 Junction/Cytoplasm Ratio	C	
Total Number of Junctions		
Percent of Stabilised Junctions		
Percent of Linear Junctions		
Percent of Jagged Junctions		
Junction Stability Index		
Cytoplasmic NICD Puncta Intensity		D
Nuclear NICD Puncta Intensity		
Total NICD Puncta Intensity		
NOTCH Activation Class		
Nuclear NICD Fraction		

Supplementary Table 1: HCIAEC parameters. Highlighted parameters (groups A-D) were used in individual PCAs (prcomp package). For each group the first 3 PCA components were selected (capturing >90% total variance for each group). 12 PCA components were used in tSNE computation (Rtsne package with pca option set to FALSE).

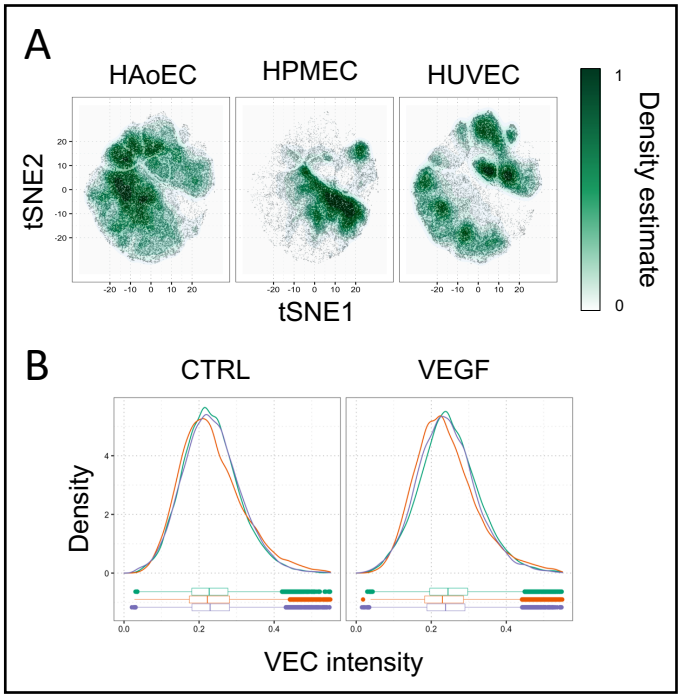

Supplementary Figure 2: A) HUVEC, HAoEC and HPMEC, density distribution of CDH5 intensities. B) HUVEC, HAoEC and HPMEC, density estimate of VEC intensity by cell type.

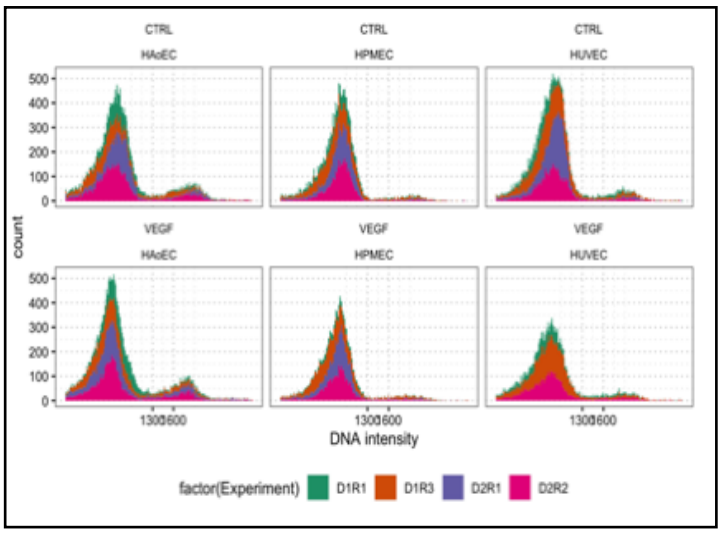

Supplementary Figure 3: HAoEC, HPMEC and HUVEC distributions of DNA intensities measurements (Coloured by experiment)

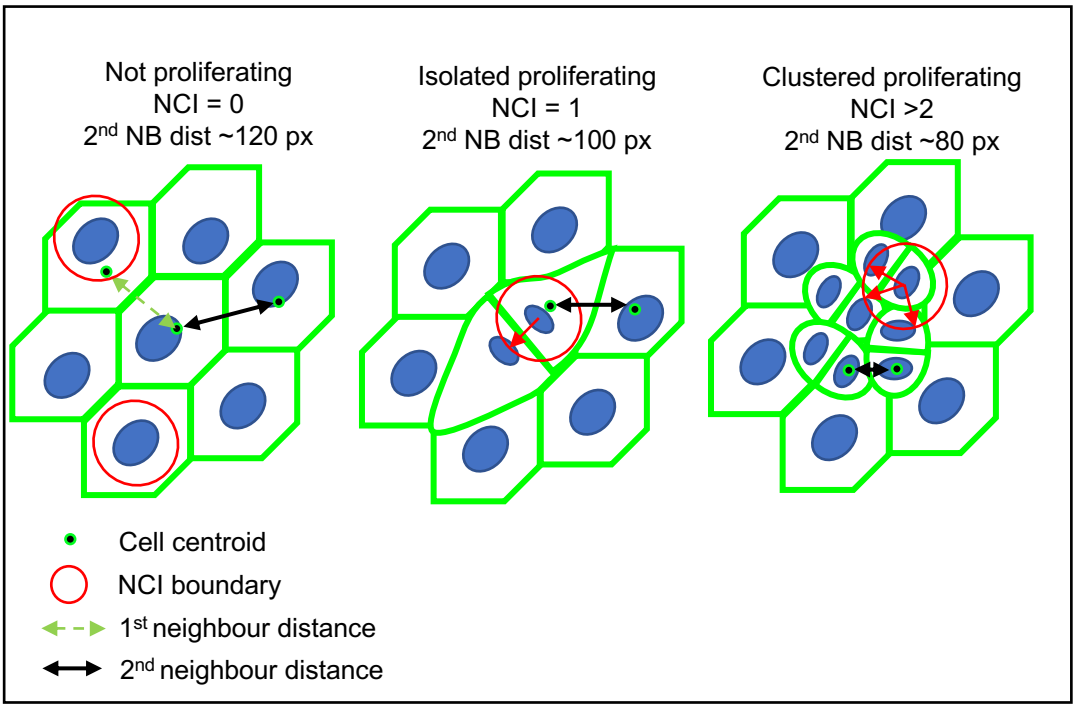

Supplementary Figure 4: Schematics representing the logic behind assessment of clonal proliferation by NCI and validation with cell 2nd NB distance. NCI = Nuclei clustering index.

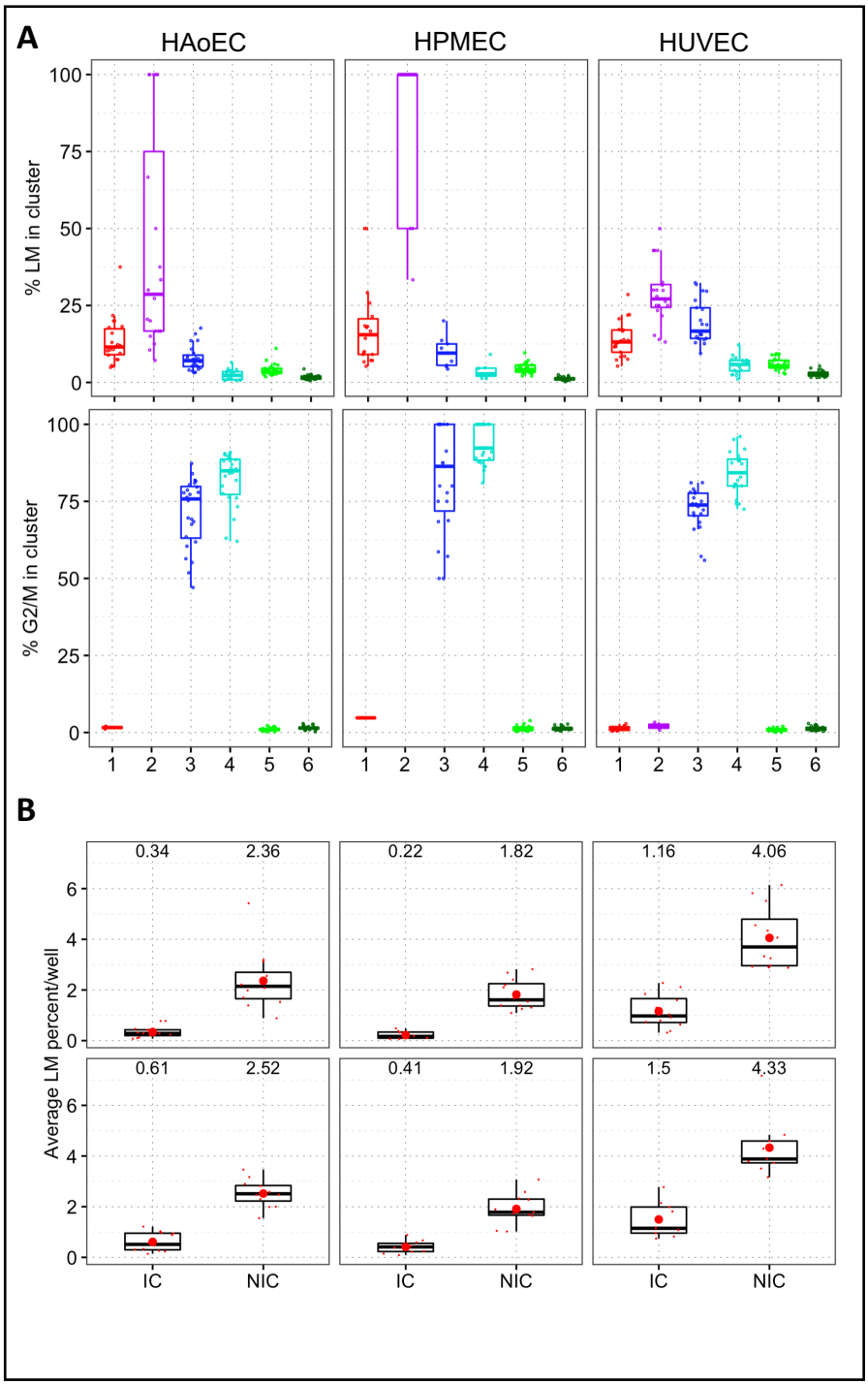

Supplementary Figure 5: A) LM and G2/M cells percentages in tSNE clusters. G2/M cells were highly enriched in clusters 3 and 4 (Nu Clustering < 2), LM cells were enriched in Cluster 2 (Nu Clustering >=2). B) Average LM number per well either in colonies (IC) or isolated (not in colony, NIC), p<0.001 for all IC-NIC comparisons.

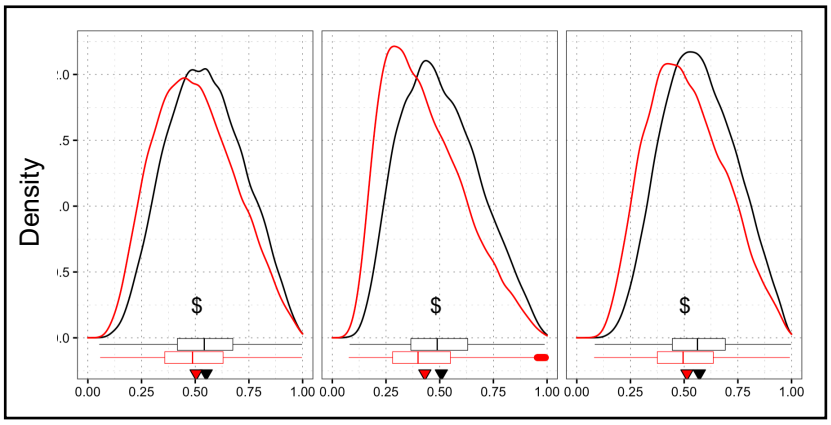

Supplementary Figure 6: HUVEC, HAoEC and HPMEC, density distributions of width to length ratio as index of cell elongation. VEGF induced significant reduction of WLR in all cell lines indicating cell elongation.

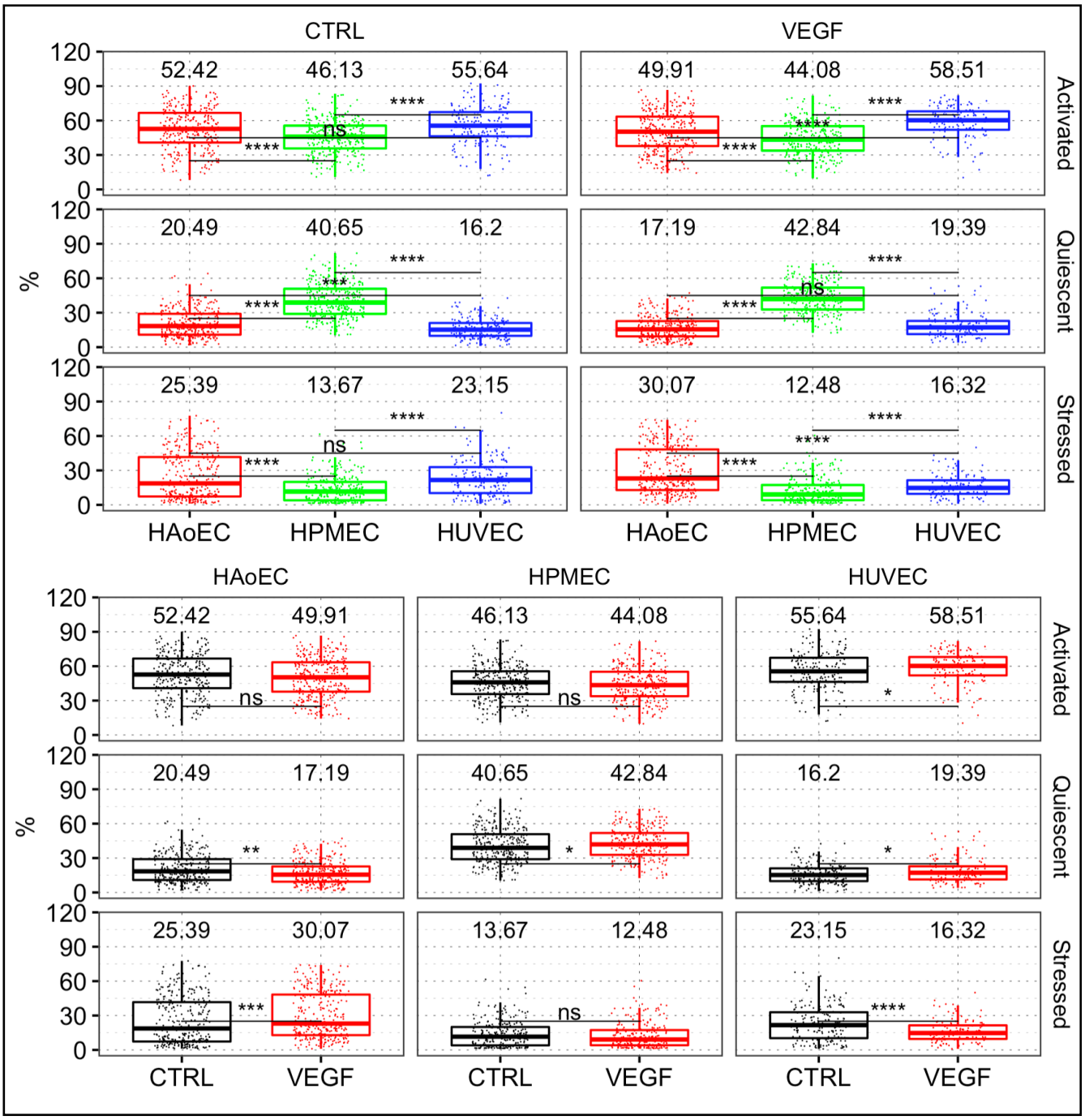

Supplementary Figure 7: HAoEC, HPMEC and HUVEC Activation classes

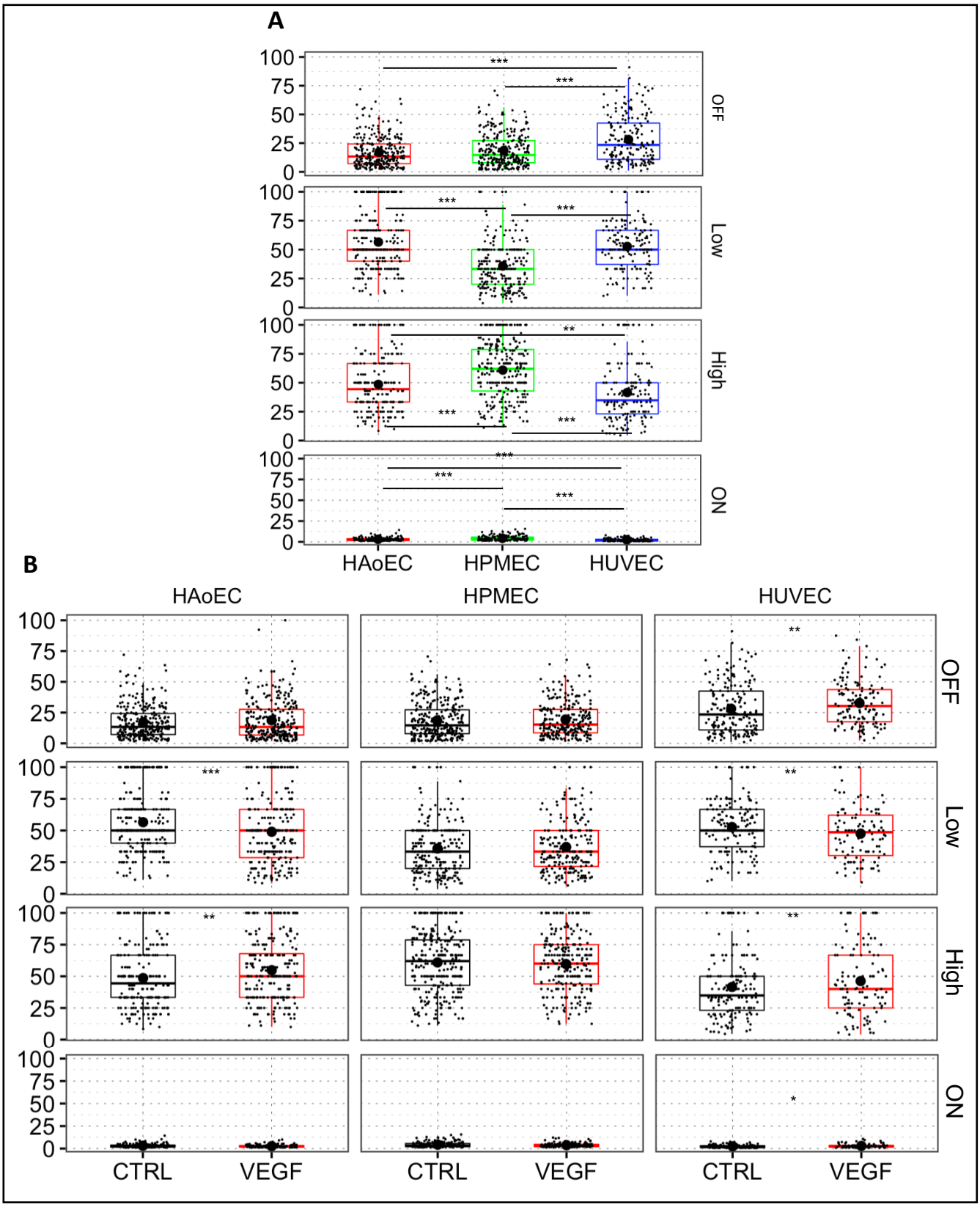

Supplementary Figure 8: HUVEC, HAoEC and HPMEC, NOTCH activation comparisons. A) Comparisons between cell types at baseline. B) Comparisons between Cell Types upon treatment with VEGF. * P<0,05, ** p<0.01, *** P<0.001

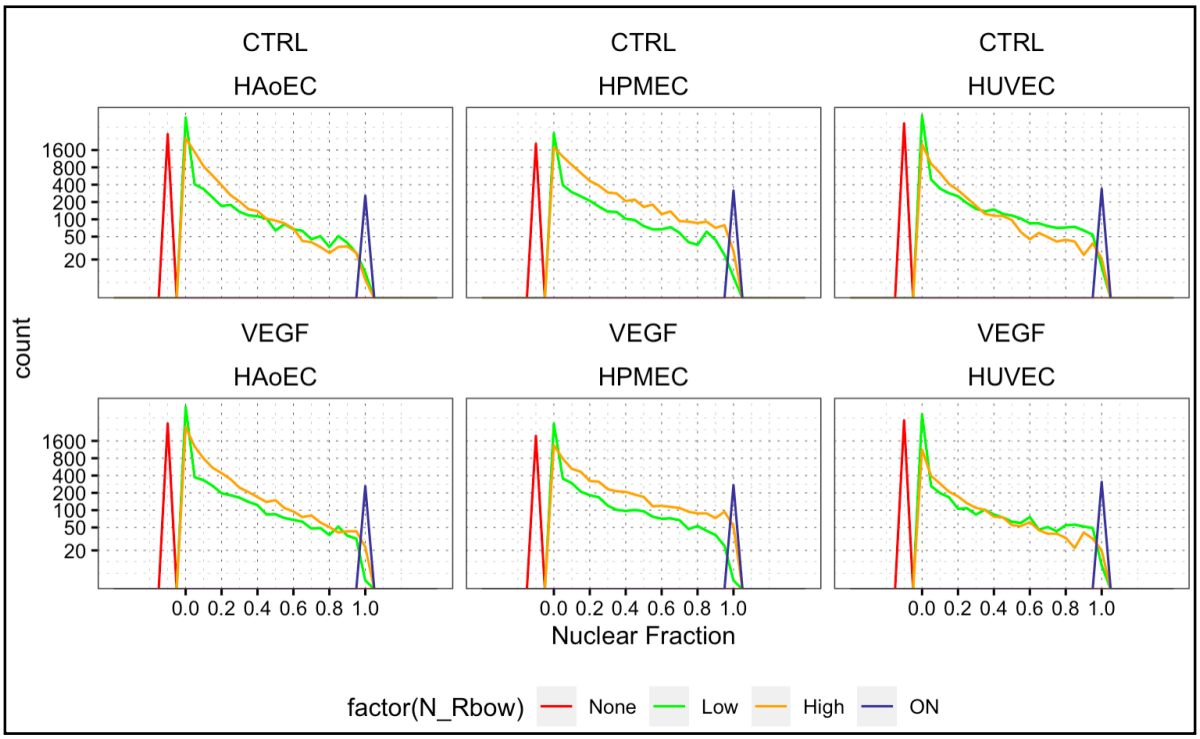

Supplementary Figure 9: HUVEC, HAoEC and HPMEC, NOTCH Nuclear fraction distribution

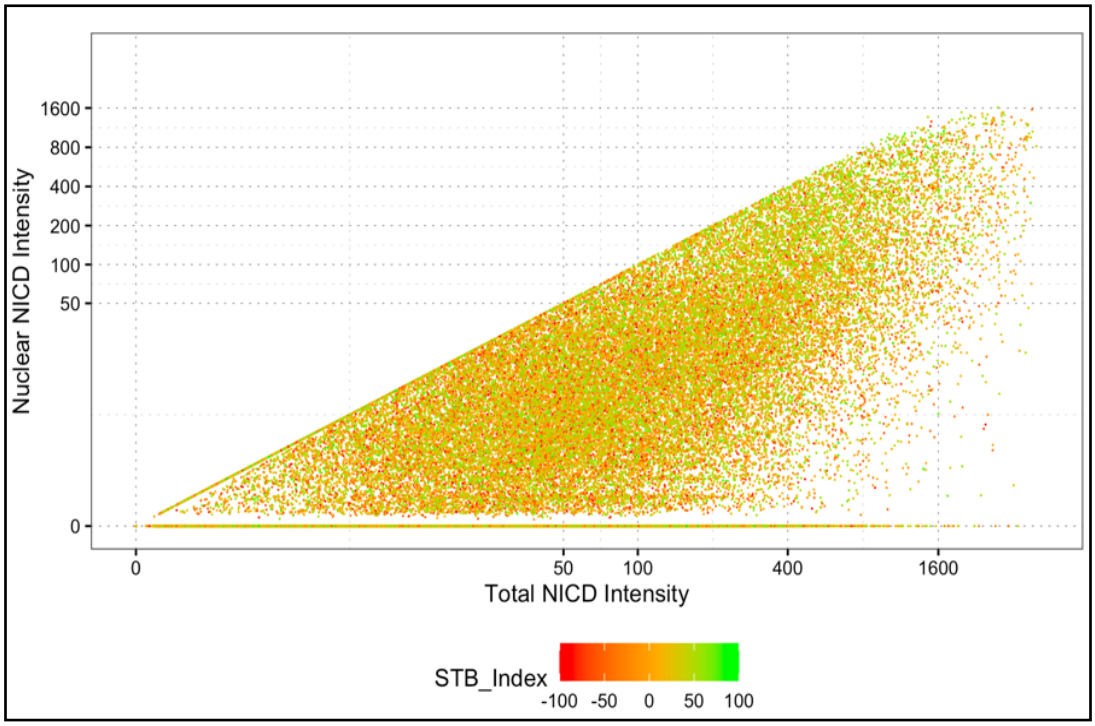

Supplementary Figure 10: HUVEC, HAoEC and HPMEC, Total NCID vs Nuclear NICD scatterplot. Coloured according to STB_Index. No correlation between NICD activity and STB index is evident.

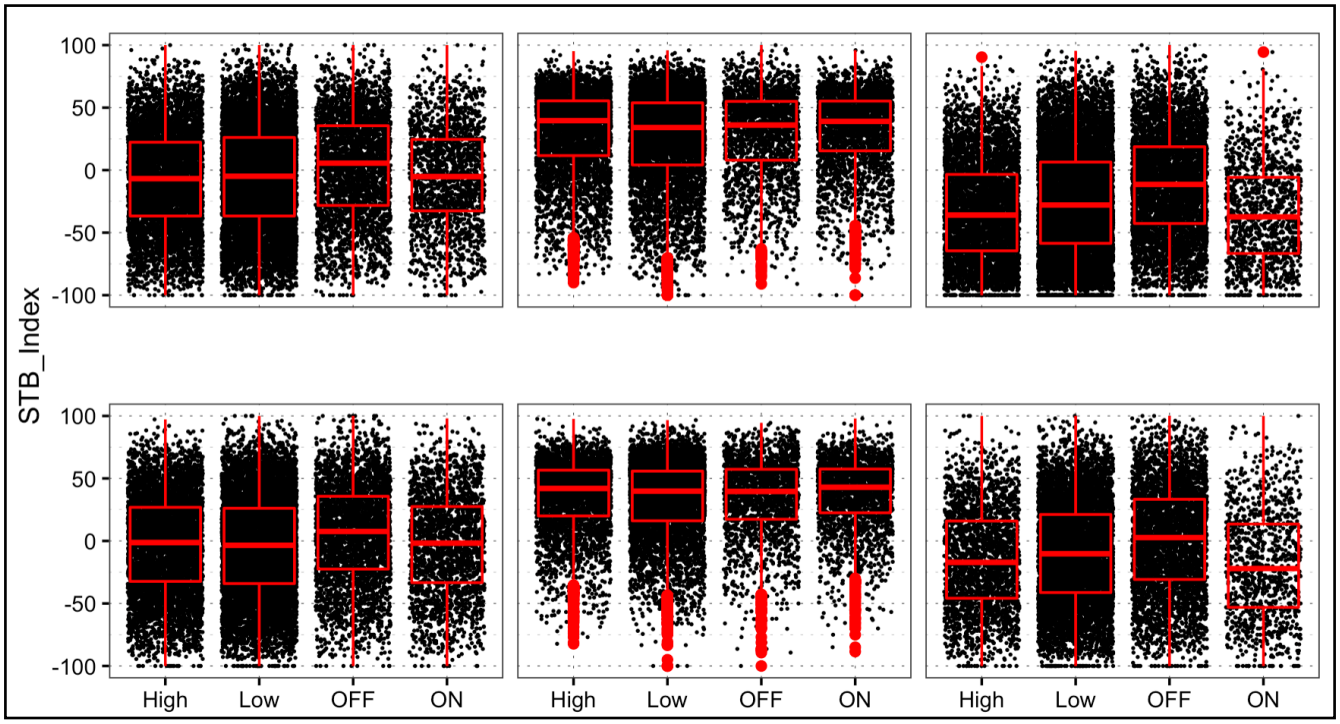

Supplementary Figure 11: HUVEC, HAoEC and HPMEC, STB index in the four NOTCH activation classes. Average stability index is similar in all classes.

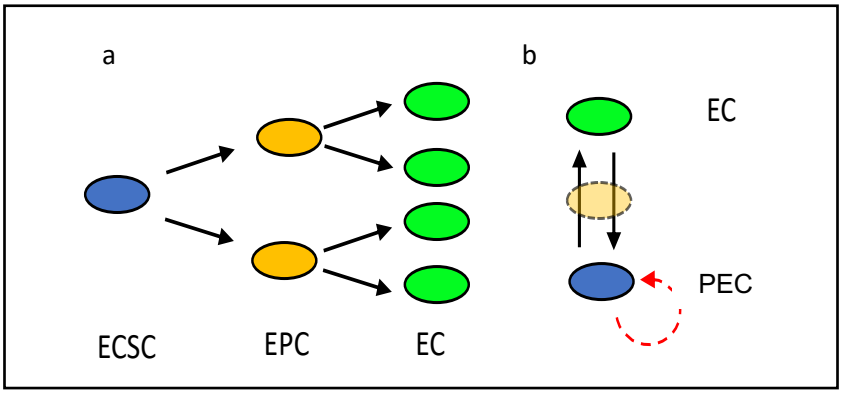

Supplementary Figure 12: Possible models of cell proliferation. a) Unidirectional model in which only endothelial cell stem cells (ECSC) and endothelial precursor cells (EPC) can proliferate while fully differentiate EC cannot proliferate. b) Cyclic model in which every EC within monolayers remains quiescent until contact inhibited. Local loss of contact in the presence or absence of supplementary stimulation (i.e. VEGF) relieve contact inhibition of proliferation and the EC can re-enter cell cycle as a proliferating EC (PEC).